STIFFNESS REDUCTION RESULTING FROM TRANSVERSE CRACKING IN FIBER-REINFORCED COMPOSITE LAMINATES

by

Alton Lee Highsmith

Thesis submitted to the Graduate Faculty of the
Virginia Polytechnic Institute and State University
in partial fulfillment of the requirements for the degree of

MASTER OF SCIENCE

in

Engineering Mechanics

APPROVED:

K. L. Reifsnider, Chairman

E. G. Henneke, II

W. W. Stinchcomb

D. Frederick, Department Head

August 1981

Blacksburg, Virginia

ACKNOWLEDGEMENTS

The author gratefully acknowledges:

--Dr. Kenneth L. Reifsnider, for his patience and encouragement throughout this investigation.

--Dr. W. W. Stinchcomb and Dr. E. G. Henneke who offered numerous helpful suggestions while serving on his committee.

--his fellow graduate students, who were willing to lend a hand whenever called upon.

-- for their assistance in the lab.

-- , who fabricated and machined the specimens.

-- , who provided his darkroom wizardry.

-- , for lending her expertise in typing the manuscript.

TABLE OF CONTENTS

LIST OF FIGURES

LIST OF TABLES

I. INTRODUCTION

One of the primary differences between the mechanical response of fiber reinforced composite laminates and that of more conventional structural materials, such as aluminum and steel, is that the damage that develops in such composites is generally much more complex. In traditional engineering materials, one particular flaw usually accounts for failure. In laminated composites, numerous defects above the atomic level but still microscopic in nature (including transverse cracking, delamination, fiber breakage, and fiber-matrix debonding) may contribute to the eventual failure of the material. In this investigation, degradation of the mechanical response of composite materials, as determined via stiffness measurements, resulting from transverse cracking is studied.

The three most important mechanical properties of structural materials are strength, stiffness, and life. Measurement of strength or life during damage development in a material is not feasible, because only one such measurement can be made for one specimen, and as yet it is very difficult to compare damage states between two specimens. On the other hand stiffness can be measured frequently during damage development, and can be measured without further degrading the material. Therefore, stiffness is a potential nondestructive test parameter which could be used to monitor the damage which develops in a component during service, and to establish residual strength and life. Numerous such applications of stiffness change as a measure of damage development have been cited in the literature [1].

Previous investigations in which stiffness, as well as other parameters such as ultrasonic attenuation and acoustic emission, were monitored during damage development, were primarily qualitative in nature [2]. With regards to transverse cracking, the most important discovery was that of the characteristic damage state. It was noticed that after sufficient loading the off-axis plies in a laminate reach a saturation state, wherein the distance between consecutive cracks in a particular ply is nearly uniform throughout the specimen. Hence, the cracking which appears in all off-axis plies in this state forms a distinctive pattern, and is referred to as the characteristic damage state (CDS). This pattern can be predicted by a shear lag analysis [3].

If transverse cracks develop in the off-axis plies in a laminate, the microscopic aspects of the deformation resulting from the application of an axial load are changed. This change in the deformation field is a result of a change of the constraints imposed on the material elements on the microscopic level. The surface of a matrix crack is a free surface, and the constraints imposed on the material near such a surface are different from the constraints imposed on the material elsewhere. Since the deformation field is altered by the presence of transverse cracks, the stress field is also altered. Because the transverse cracks reach a reproducible saturation pattern (CDS), one such arrangement of cracks can be analyzed in detail in order to predict the effect of the CDS on global laminate mechanical response. Several such analyses have appeared in the literature and are discussed briefly in Section 2. However, this is a rather cumbersome analytical procedure. A simpler analysis can be arrived at if one considers only the effect the damage

has on the average stress sustained by each ply instead of the fully detailed stress field. Damage changes the apportionment of the applied load among the constituent plies. In a laminate analysis, an applied load is apportioned using the plies in proportion to their respective stiffnesses; one way to simulate the redistribution of stress caused by damage development is to use a laminate analysis and adjust the lamina properties of damaged plies appropriately. One of the objectives of this investigation was to determine the effect of the CDS on laminate mechanical response. This simple analysis provides global laminate stiffnesses in the damage state which is an indicator of laminate response.

Because composite laminates are typically anisotropic and non-uniform, several stiffness components are required to completely describe their mechanical response. In fact, six extensional stiffness components, six bending stiffness components, and six bend-extension coupling stiffness components are required in the most general case. Structural designs may depend on several of these stiffnesses. In addition, a long term goal is to be able to both classify and quantify damage in a composite laminate. Since the three principal damage modes, transverse cracking, delamination, and fiber breakage, may all contribute to the degradation of the mechanical response of the laminate, no single stiffness measurement will suffice even to classify the damage. In order to more fully understand the effect of transverse cracking on the mechanical response of laminates to multiaxial loadings, several stiffness components (E_{xx}, ν_{xy}, G_{xy}, and D_{yy}) were monitored before and after damage development.

This study is the quantitative extension of previous work [4,5]. After obtaining considerable insight into the physics of the problem, relationships (not merely trends), between crack density and stiffness were sought. One of the first difficulties to be overcome was that in the previous studies, axial behavior was so dominated by the 0 deg plies that laminate stiffness changes were small. For this investigation, $[0,90_3]_s$, $[90_3,0]_s$, $[0,90]_s$, and $[0,\pm45]_s$ glass-epoxy laminates (type I,II,V, and IV materials respectively) were studied. A glass-epoxy material system was chosen because the ratio of transverse to longitudinal moduli for a lamina (E_2/E_1) for this material is large in comparison to that of other advanced composites. The laminate load carried by off-axis plies, particularly 90 deg plies, is significant, and stiffness changes resulting from transverse cracking in these situations will also be significant. And while the first two laminates listed may not be of great practical value, their stiffness changes due to cracking are large enough to provide a critical test for an analysis, and also to allow a check for stacking sequence dependence. The remaining two laminates provide different constraint cases and different off-axis plies to further test the analysis.

II ANALYSIS

2.1 Introductory Remarks

Numerous attempts to form a stress analysis of a composite laminate with transverse cracks in off-axis plies are found in the literature. The various analyses differ considerably in complexity. Generally, the simpler models do not provide detailed information about local disturbances in the deformation field, while the more sophisticated analyses are limited to very simple geometries and loading configurations. Three types of analyses are found: approximate solutions to the field equations, exact solutions to approximate equations, and modified laminate analyses.

Analyses that are approximate solutions to the exact field equations are numerical solutions to the equations of equilibrium. The most popular numerical solution schemes are the finite element and finite difference methods. While the finite difference method is better able to meet certain boundary conditons, the finite element method can be more easily applied to irregular geometries. Wang et al. [6,7] have developed a finite element analysis that predicts the saturation spacing of transverse cracks in a 90 deg ply within a laminate. First, the strain energy release rate associated with the formation of a single transverse crack in the 90 deg is calculated using a crack closure method. Then they postulate that saturation spacing is that spacing at which the strain energy release rate associated with the formation of a second crack is equal to that associated with the formation of the first crack. Talug [8] has developed a finite difference analysis of an

eight ply symmetric laminate with a transverse crack that crosses one or more plies. Talug's analysis determines the distributions of all six stress components in the vicinity of the transverse crack.

Vasil'ev et al. [9] have derived a closed form solution to simplified versions of the governing equations for a $[0,90]_s$ laminate with a transverse crack in the 90 deg plies subjected to a load in the 0 deg direction. In this analysis it is assumed that the interlaminar-normal stress is zero throughout the damaged laminate, and that because the plies are thin, the in-plane stresses do not vary across the thickness of a given ply. The $[0,90]_s$ laminate has no in-plane shear stress (τ_{xy}) which simplifies the governing equations. This analysis predicts distributions of the two in-plane normal stresses and the interlaminar shear stress as a function of distance from the crack in both the 0 deg and 90 deg plies.

The approximate field equations that are most commonly used to model a composite laminate with transverse cracks in off-axis plies are those obtained using an equilibrium element approach using a so-called shear lag analysis. Such a treatment is one-dimensional in nature. A shear lag analysis was first applied to composite laminates by Zweben [10] to model the strength of notched laminates. Several investigators have applied shear lag analyses to the transverse cracking problem. Garrett and Bailey [11], Parvizi and Bailey [12], and Plunkett [13] have made use of a shear lag analysis that tacitly assumes a parabolic distribution of normal stress across the thickness of each ply to predict crack density as a function of applied load. Garrett and Bailey make further

use of the analysis to predict the axial stress vs. strain response of cross ply glass-polyester laminates during damage development. These analyses are limited to symmetric laminates made up of plies of alternating orientation. Reifsnider [3] has developed a shear lag model that assumes the existence of a thin shear transfer region between adjacent plies. This analysis can be performed on laminates of more complex stacking sequences.

One can also approach the problem with a modified laminate analysis, a simpler model of the mechanical response of a laminate with transverse cracks in off-axis plies. Here, the stiffnesses of the damaged plies are reduced and a laminate analysis is performed. Total ply discount, whereby all lamina stiffnesses of a damaged ply are reduced to zero, and mode limited discount, whereby the transverse and shear stiffnesses are reduced to zero in damaged plies, are two techniques for systematically adjusting lamina properties in order to predict the mechanical properties of a damaged laminate [14]. The advantage of a modified laminate analysis is that it predicts multiaxial mechanical properties for a damaged laminate.

More detailed discussions of Talug's finite difference analysis, Reifsnider's shear lag analysis, and a modified laminate analysis follow.

2.2 Finite Difference Analysis

In order to determine how transverse cracking in off-axis plies affects the stiffness of the overall laminate, the stress state in the vicinity of such cracks must be found. Talug [8] has formulated a finite difference solution to such a problem. The laminate is assumed to be symmetric and infinite in width (the y direction). The x-axis is chosen to be the load direction, and the z-axis is chosen through the thickness, with z=0 at the midplane. The finite difference discretization was performed on the first quadrant of the X-Z plane. The discretized governing equations that were obtained were fully second order, both on the boundaries and in the interior.

The principle reason for using this technique is that it yields a full-field solution; all six stress components are determined throughout the laminate in the presence of a crack. One can then determine the distance from the crack over which the stresses in the x-y plane are redistributed to reach essentially laminate analysis values. Also, the out of plane stresses σ_z, τ_{xz}, and τ_{yz}, stresses which may initiate delamination, are determined in the vicinity of a crack. To illustrate the capabilities of the finite difference analysis, stress distributions in a $[0,\pm45,90]_s$ graphite epoxy laminate with a transverse crack in the 90 deg ply that were determined by Talug [8] and are shown in Figs. 1 and 2. Lamina properties are shown in Table 1. Figure 1 shows the through the thickness variation of normal stress σ_x in damaged and undamaged laminates. Stress concentration factors can easily be obtained from such data. Figure 2 is a contour map of the interlaminar

Table 1. Material properties for AS/3501 graphite-epoxy (V_f = 0.6).

Material	E_1 (Msi)	E_2 (Msi)	ν_{12}	G_{12} (Msi)	G_{23} (Msi)	Ply Thickness (in.)
Gr/Ep	20.6	1.43	0.30	0.65	0.49	0.005

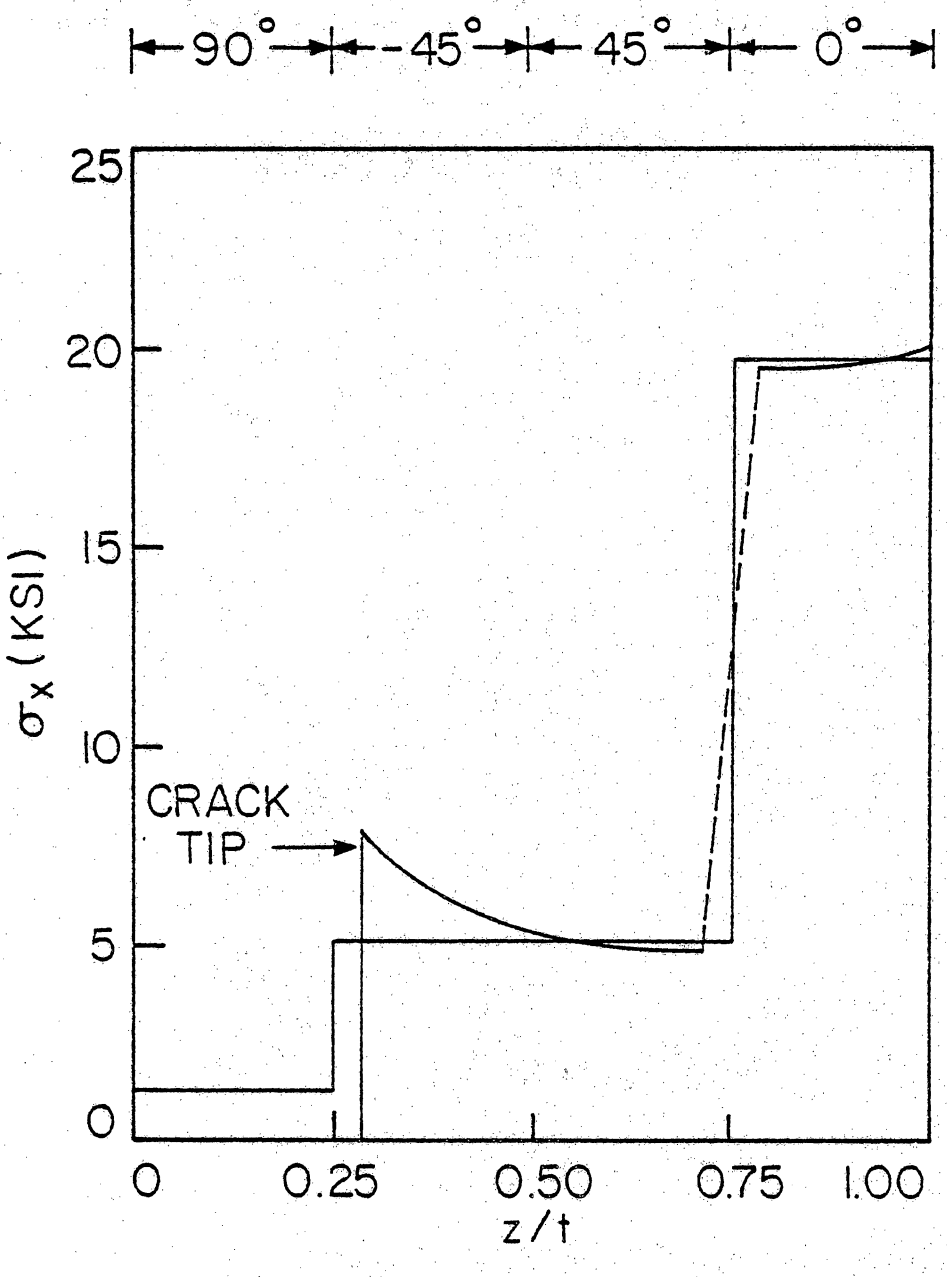

Fig. 1 Through-the-thickness variation of σ_x for a $[0,\pm45,90]_s$ graphite-epoxy laminate with and without 90° ply damage.

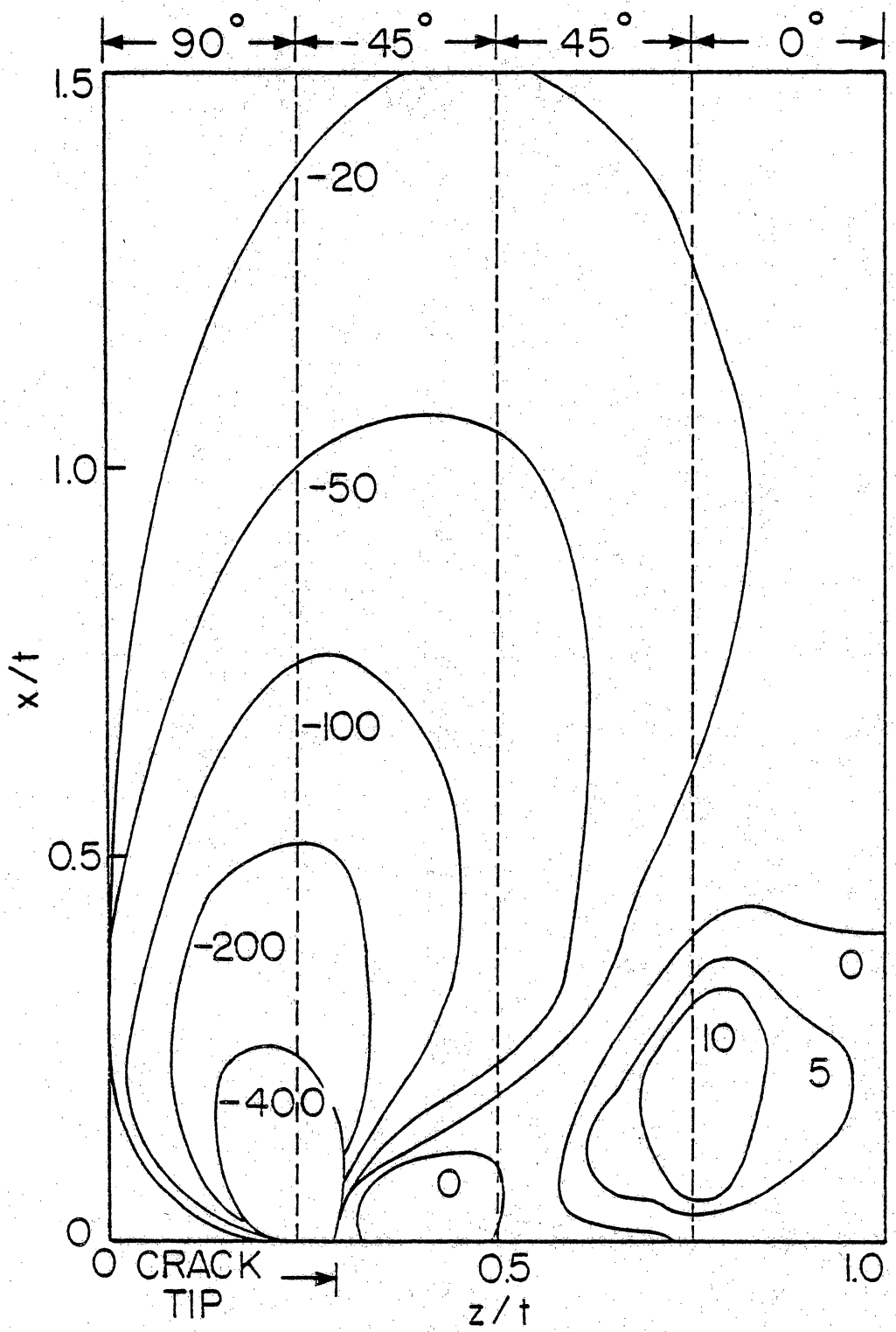

Fig. 2 Contours of τ_{xz} (psi) for a $[0,\pm45,90]_s$ graphite-epoxy laminate with 90° ply damage.

shear stress τ_{xz} for the damaged laminate. If one is to determine the precise nature of damage propagation and crack growth into adjacent plies, such a full field solution is essential.

Application of the finite difference solution is somewhat limited. Currently, the analysis cannot be applied to laminates that have transverse cracks in the outermost ply. In addition, the method is unable to analyze laminates with multiply cracked off-axis plies. And due to the large core requirements for the solution of the resulting algebraic equations, a computer implemented solution is limited to relatively simple laminates. In our case, Talug's numerical solution can analyze symmetric laminates of no more than eight plies. Further, with the discovery of the characteristic damage state it is unnecessary to know all of the details of the stress field, as it is unnecessary to know the precise details of crack growth throughout the laminate.

2.3 Shear Lag Analysis

Reifsnider [3] has developed a one-dimensional model which can approximate normal stress in the load direction, σ_x, in the various plies of a cracked laminate. Careful examination of crack patterns in specimens of various materials shows that shear deformations in any given ply are restricted to a thin region in the vicinity of interfaces of that ply with adjacent plies. Further, this region tends to be resin-rich, and thus is less stiff in response to shear loads than the central portion of the lamina. Transverse cracks extend up to this region, but usually do not extend into it. In the one-dimensional model that follows, this thin region is assumed to be a shear transfer region.

Figure 3 shows a typical one-dimensional equilibrium element for a ply within a laminate, ply i. The thickness of the ply is a_i, the thickness of the shear transfer region is a material constant b; in the figure, the ply is shown to be cracked. At a crack surface, the stress in the ply is zero, but away from the crack, the stress is non-zero; load is transferred back into the middle ply i from the constraining plies i-1 and i+1 via shear transfer across the thickness b. The equilibrium equation for such a ply is

$$a_i E_i \frac{d^2 U_i}{dx^2} - \frac{2G}{b}(U_i - U_{i-1}) - \frac{2G}{b}(U_i - U_{i+1}) = 0 \qquad (1)$$

where E_i is the longitudinal modulus of the middle ply, G is the shear modulus in the shear transfer region, and U_{i-1}, U_i and U_{i+1} are the displacements in plies i-1, i, and i+1, respectively. There are two special cases of Eqn. (1) which need to be considered. Suppose ply i is an exterior ply of a laminate, so that there is no ply i-1 to constrain it. Then the shear lag contribution from ply i-1, $\frac{2G}{b}(U_i - U_{i-1})$, must be eliminated from (1), since the left surface of ply i is a free surface. The resulting equation is

$$a_i E_i \frac{d^2 U_i}{dx^2} - \frac{2G}{b}(U_i - U_{i+1}) = 0 \qquad (2)$$

The other special case arises when one surface of ply i is the midplane of a symmetric laminate. For example, if plies i and i-1 are plies on either side of the midplane of such a laminate, then $\frac{2G}{b}(U_i - U_{i-1}) = 0$ from symmetry, since $U_i = U_{i-1}$. This result yields an equation which is identical to that which was obtained for an exterior ply. Equations (1)

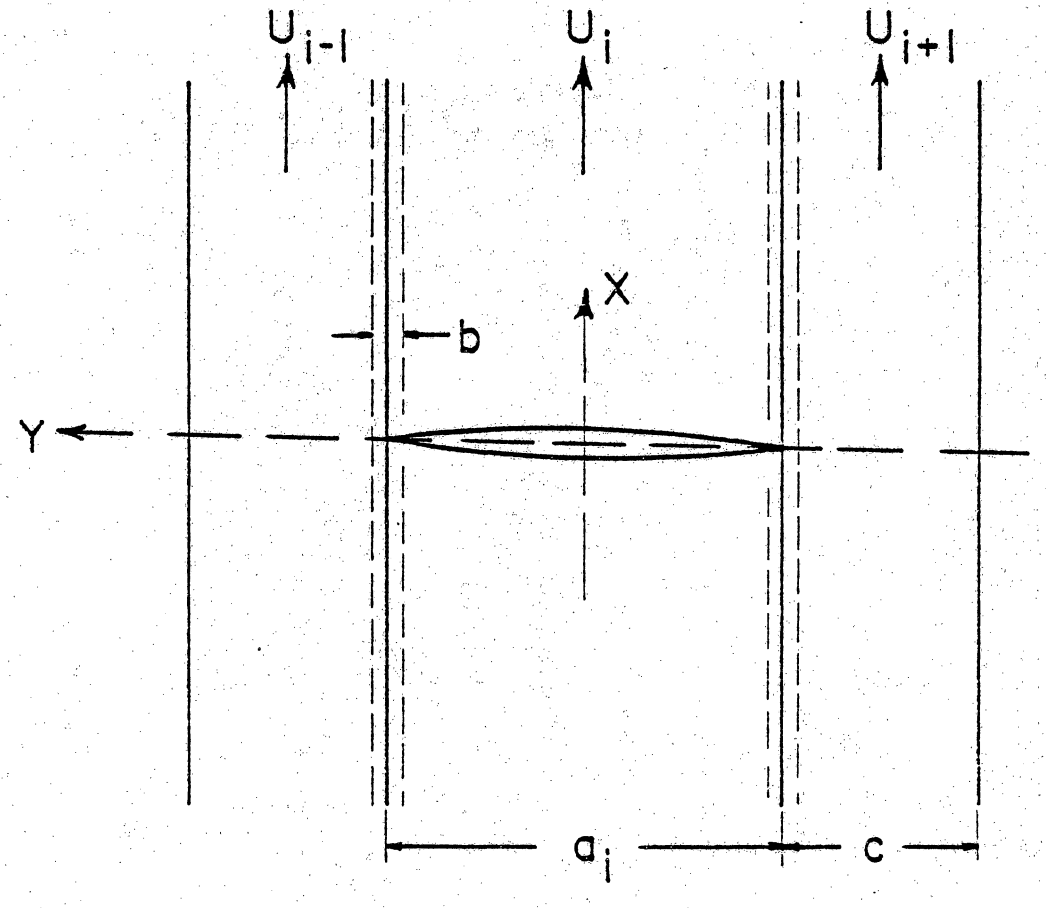

Fig. 3 Equilibrium element used in the formulation of the shear lag model.

and (2) can be rearranged into a form more convenient for manipulation by dividing through by $a_i E_i$. By defining k_i such that

$$k_i = \frac{2G}{b a_i E_i} \tag{3},$$

Eqn. (1) can be written in the form

$$k_i \left(-U_{i-1} + 2U_i - U_{i+1}\right) - \frac{d^2 U_i}{dx^2} = 0 \tag{4},$$

and Eqn. (2) can be written in the form

$$k_i \left(U_i - U_{i+1}\right) - \frac{d^2 U_i}{dx^2} = 0 \tag{5}.$$

When an entire laminate is analyzed by the shear lag model, an assembly of second order differential equations must be solved simultaneously. These differential equations are the equilibrium equations for the constituent plies. If the laminate is symmetric, only one of the symmetric halves of the laminate need be analyzed. In an analysis of n plies the assembled equations can be written in vector form as

$$\begin{bmatrix} k_1 & -k_1 & 0 & 0 & 0 & \dots & 0 \\ -k_2 & 2k_2 & k_2 & 0 & 0 & \dots & 0 \\ & & & & & & \\ \vdots & & & & & & \\ 0 & 0 & 0 & 0 & \dots & -k_n & k_n \end{bmatrix} \left\{ U \right\} - \left\{ \frac{d^2 U}{dx^2} \right\} = \left\{ 0 \right\} \tag{6}.$$

This system of equations is similar in nature to those obtained for coupled oscillator problems, and the solutions take the form of sums of

characteristic solutions multiplied by arbitrary constants. A solution of the form

$$\{U\} = e^{\alpha x}\{v\} \tag{7}$$

where $\{v\}$ is constant is assumed, so

$$\left\{\frac{d^2U}{dx^2}\right\} = \alpha^2 e^{\alpha x}\{v\} \tag{8}.$$

Substituting Eqns. (7) and (8) into Eqn. (6), combining terms and dividing by the exponential term yields

$$\begin{bmatrix} (k_1-\alpha^2) & -k_1 & 0 & \cdots & 0 \\ -k_2 & (2k_2-\alpha^2) & -k_2 & \cdots & 0 \\ & & & & \\ \vdots & & & & \\ 0 & \cdots & & -k_n & (k_n-\alpha^2) \end{bmatrix} \begin{Bmatrix} v \end{Bmatrix} = \begin{Bmatrix} 0 \end{Bmatrix} \tag{9}.$$

For non-trivial solutions, α^2 is an eigenvalue and $\{v\}$ is the corresponding eigenvector of the matrix

$$[k] = \begin{bmatrix} k_1 & -k_1 & 0 & \cdots \\ -k_2 & k_2 & -k_2 & \cdots \\ & & & \\ \vdots & & & \\ 0 & \cdots & -k_n & k_n \end{bmatrix} \tag{10}.$$

Such a matrix has n eigenvalues and n corresponding eigenvectors. Because of the form of the matrix,

$$(\alpha_1)^2 = 0, \quad \{v\}_1 = \begin{Bmatrix} 1 \\ 1 \\ 1 \\ \cdot \\ \cdot \\ \cdot \end{Bmatrix}$$

are always an eigenvalue and corresponding eigenvector. The most general solution is a linear combination of the n simple solutions, so the displacement vector can be written in the form

$$\{U\} = \left(C_1 + D_1 X\right)\{v\}_1 + \sum_{\ell=2}^{n}\left(\left(C_\ell e^{\alpha_\ell x} + D_\ell e^{-\alpha_\ell x}\right)\{v\}_\ell\right) \qquad (11),$$

where C_ℓ and D_ℓ are arbitrary constants.

The analysis is completed by imposing boundary conditions at the ends of the laminate. The displacements at the ends of uncracked plies are fixed. Cracked ply conditions are imposed at the ends by requiring the normal stress to be zero in the cracked ply. If a laminate is analyzed that is semi-infinite in the x direction, the strain must be bounded as x becomes infinite. The imposition of boundary conditions determines the arbitrary constants C_ℓ and D_ℓ.

The primary difficulty involved in implementing this shear lag analysis is determining values for the shear stiffness (G) and thickness (b) of the shear transfer layer for a given material system. In a previous investigation [2], for the graphite-epoxy system used in the finite difference method in Section 2.2, the properties used were G = 0.20 Msi, b = 0.0005 in. The recent development of a moiré interferometry apparatus has provided a method for experimentally determining (G/b), and such a determination for the glass-epoxy system used in the

experimental program of this investigation is illustrated in Appendix I. By analysis of a moiré fringe pattern from a $[0,90_3]_s$ specimen, a value of (G/b) = 50 Msi/in. was determined for the glass-epoxy system.

In order to evaluate the shear lag model, stress distributions predicted by the shear lag model were compared with those predicted by the finite difference model. Two graphite-epoxy laminates with transverse cracks in the 90 deg plies were analyzed. One laminate had a stacking sequence of $[0,\pm45,90]_s$ and the other laminate had a stacking sequence of $[0,90,\pm45]_s$. For the finite difference model, an aspect ratio of L/T = 6 was used, where T is the laminate half-thickness. The material properties used were those shown in Table 1. Semi-infinite laminates were investigated via the shear lag model. The transverse cracks were placed in the 90 deg plies at X/T = 0. The distributions of interlaminar shear stress τ_{xz} in the x-directions along the -45,90 interface (the stress that--according to the shear lag model--accounts for the transfer of load back into the damaged ply) predicted by the two analyses for the $[0,\pm45,90]_s$ laminate are shown in Fig. 4. The distributions are of the same general shape. Better agreement between the two models could be obtained by modifying the shear stiffness and thickness of the shear transfer layer used in the shear lag model. These two parameters were obtained from available physical data; no curve fit was performed. Figure 5 shows the predicted distributions of normal stress σ_{xx} in the x-direction in the 90 deg ply. The finite difference results indicate that there is a through-the-thickness gradient of normal stress. Both models indicate that the stress level becomes constant at approximately

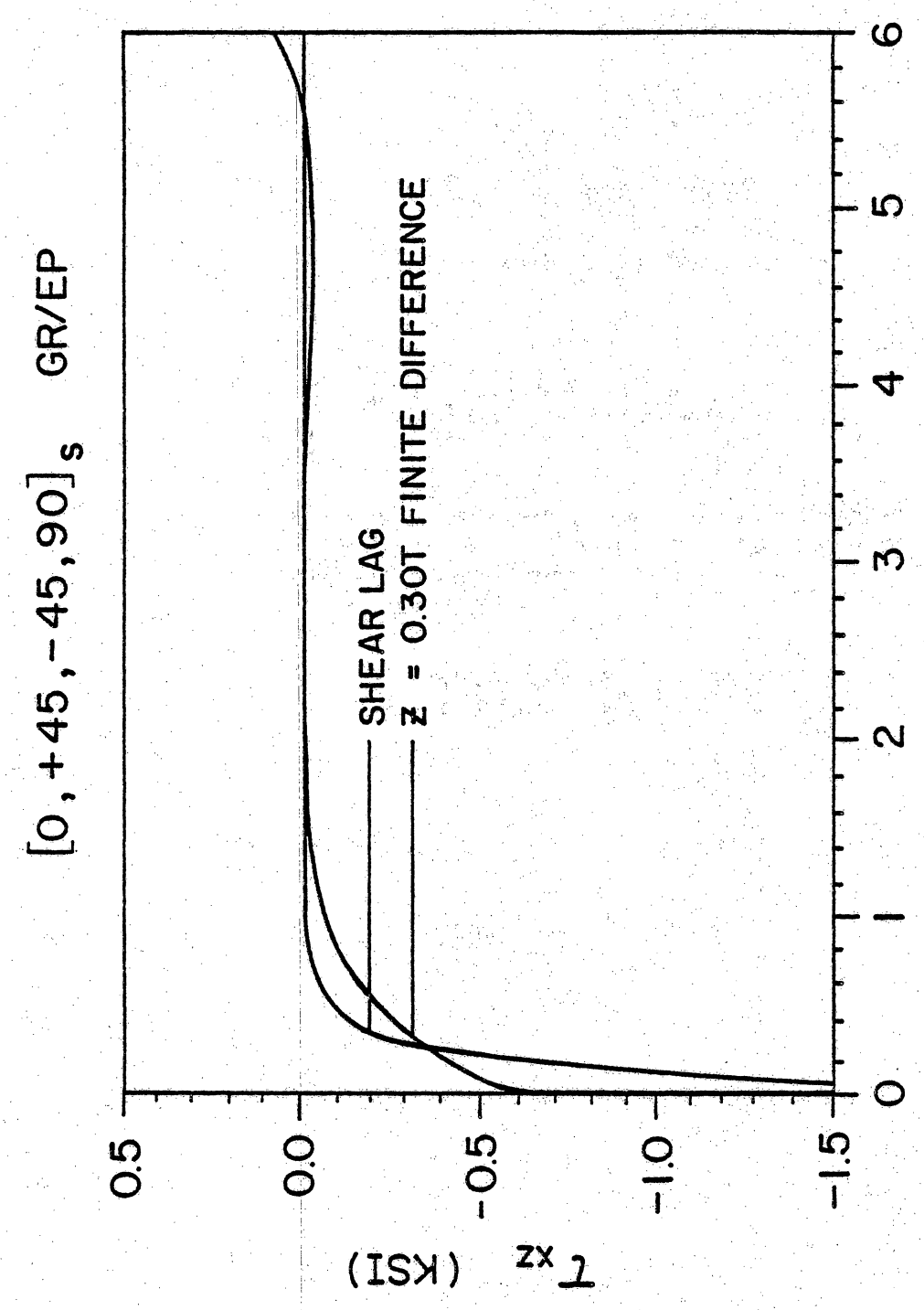

Fig. 4 Predicted distributions of τ_{xz} at the -45,90 interface of a $[0,\pm45,90]_s$ graphite-epoxy laminate with cracked 90° plies.

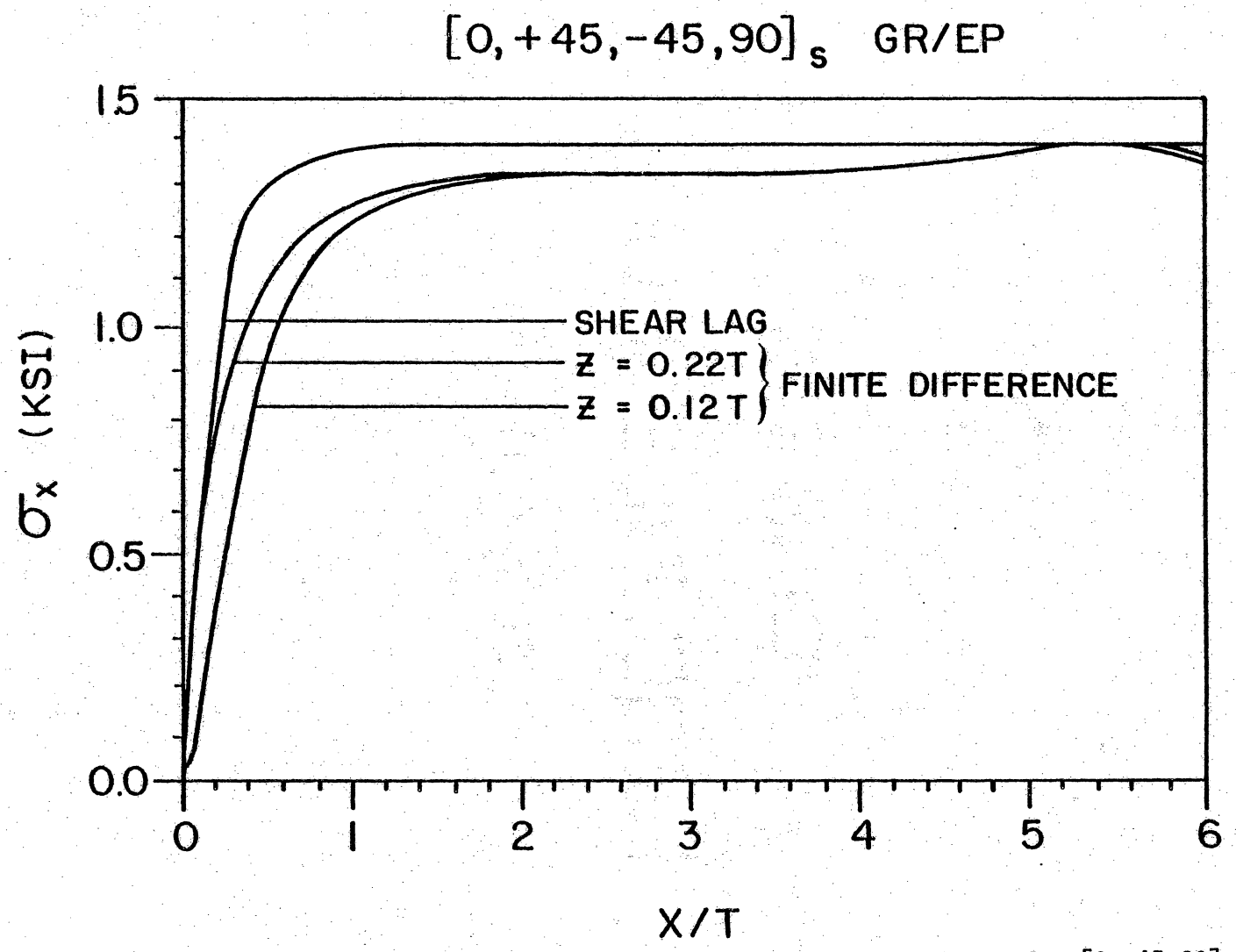

Fig. 5 Predicted distributions of σ_x in the cracked 90° plies of a $[0,\pm45,90]_s$ graphite-epoxy laminate.

X/T = 1.5. Figure 6 indicates that similar trends exist in the predicted normal stress distributions in the cracked 90 deg plies of the $[0,90,\pm45]_s$ laminate. Note that due to the different constraint imposed on the 90 deg plies, a stable stress load is reached at X/T = 1.0, which is only two thirds of the distance from the crack determined in the previous case. Overall, the agreement of the two models is good.

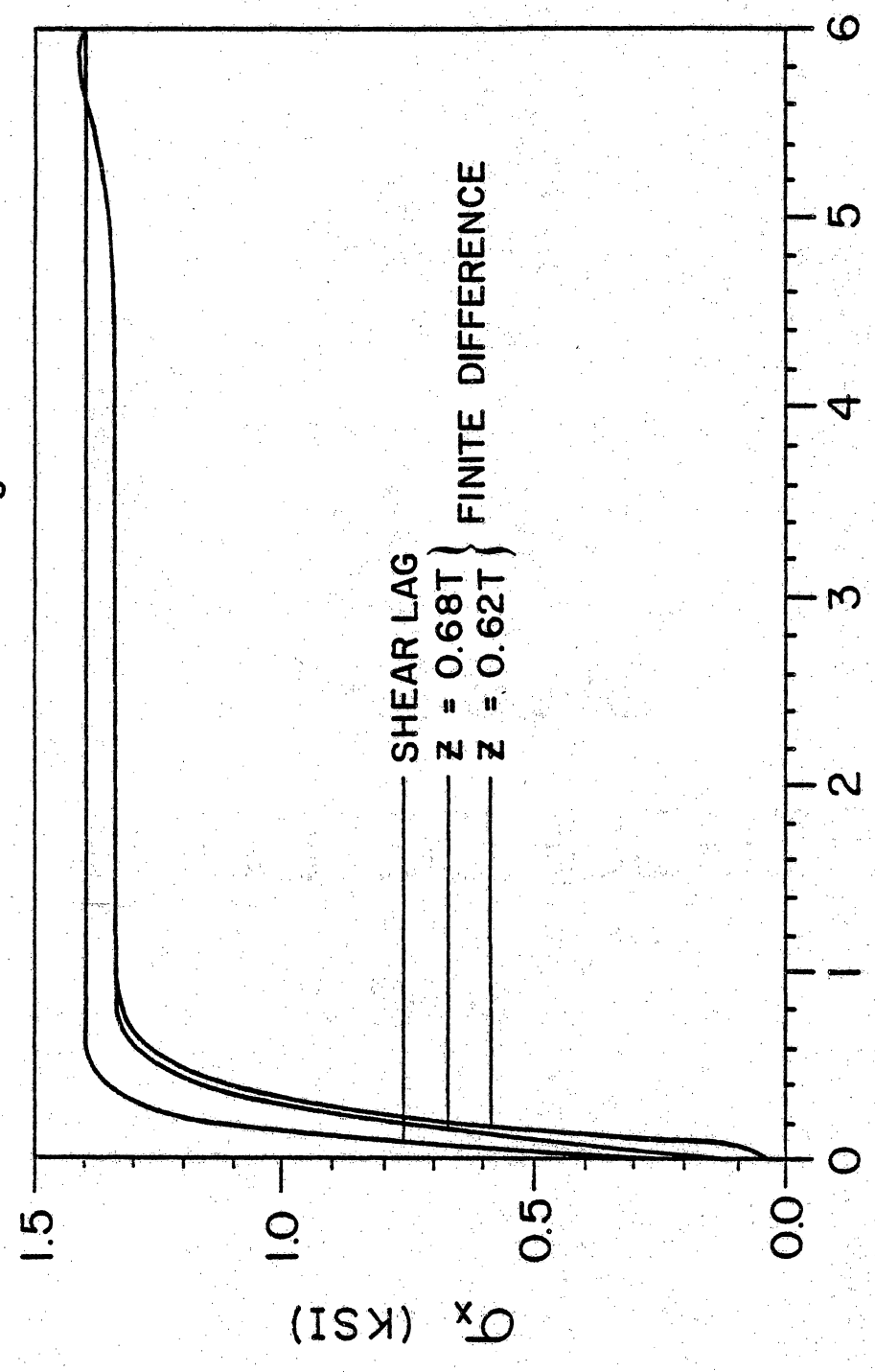

Fig. 6 Predicted distributions of σ_x in the cracked 90° plies of a $[0,90,\pm45]_s$ graphite-epoxy laminate.

2.4 Modified Laminate Analysis

If an analysis predicts the details of the stress and strain distributions in a damaged laminate, then average values of stress and strain must be calculated in order to determine how the damage affects global laminate response. The details required to analyze damage development and crack growth are not required for that determination. The details of the stress and strain fields that are essential for analyzing damage development are not as important for analyzing the effect of damage on global laminate response. A simpler model of the effect of damage on global laminate response can be constructed using a modified laminate analysis.

Both the finite difference and shear lag models indicate that when transverse cracks develop in an off-axis ply, if the laminate is subjected to a given load, the average stress in that off-axis ply is lower in the damaged state than in the undamaged state. Analytically, this decrease in average stress is a result of the imposition of a free surface boundary condition within the cracked ply. The presence of such a surface causes a change in the local constraint imposed on the material.

When the mechanical response of a composite is modeled with a laminate analysis, it is assumed that the plies are perfectly bonded together [15]; if the laminate is subjected to some loading, the strains in adjacent plies are equal at the ply interfaces. Hence, the mechanical response of the laminate is deformation controlled. This means that each ply carries a portion of the applied load that is proportional to its stiffness. One way to simulate the global response of a laminate

with transverse cracks in off-axis plies is to use a laminate analysis in which the properties of the damaged ply have been adjusted so that the laminate analysis predicts the appropriate average stresses in the damaged ply. The advantage of such an analysis is that it provides tensor stiffnesses for the damaged laminate. Laminate analysis provides extensional, bending, and bend-extension coupling stiffness. In the strictest sense, this collection of stiffness components does not constitute a tensor. The word tensor is used here to indicate that the mechanical response of a laminated composite is described by several stiffness components.

In order to implement a modified laminate analysis some systematic method for adjusting the lamina stiffnesses of damaged off-axis plies must be developed. A transverse crack is a matrix crack that is parallel to the fibers. The imposition of free surface conditions affects the stresses normal to the crack in a cracked ply. It is possible to analyze the stresses in a cracked ply in a laminate using the shear lag model, and thus determine an appropriate reduction in E_2, but in this investigation E_2 was set to zero for cracked plies in order to analyze a laminate that has reached its CDS. Although matrix cracking may influence the other lamina properties, in the modified laminate analysis used in this investigation, the in-plane lamina properties, E_1, ν_{12}, and G_{12} of the damaged plies were not adjusted. Rail shear results for type I,II, and V laminates indicated that G_{12} should not be adjusted for the cases studied. This implies that the constraint imposed on cracked plies by the adjacent plies does not allow sufficient relaxation

of shear strain in the vicinity of the cracks to have a significant effect on laminate response, but as yet no micromechanical model has been developed that supports such an argument.

III. EXPERIMENTAL PROGRAM

3.1 Introductory Remarks

The primary objective of the experimental program was to obtain physical data relating the degradation of laminate stiffness to the development of transverse cracks. In previous investigations in which such data was gathered for various graphite-epoxy and boron-epoxy laminates, only small stiffness changes resulting from transverse cracking were measured. Those material systems were so fiber dominated that overall laminate response was insensitive to matrix failures. Consider a $[0,90]_s$ graphite-epoxy laminate. Typical lamina stiffnesses for such a material system are E_1 = 20.0 Msi, E_2 = 1.5 Msi. A rule of mixtures analysis indicates that in the undamaged state the 90 deg plies carry only 7.0 percent of a load applied in the x direction. This means that if transverse cracking were to completely destroy the 90 deg plies, the laminate stiffness E_{xx} would be decreased by only 7.0 percent. A $[0,90]_s$ laminate made from a glass-epoxy system (E_1 = 6.0 Msi, E_2 = 1.5 Msi) is not so fiber dominated. A rule of mixtures analysis indicates that in this case complete degradation of the 90 deg plies would result in a 20.0 percent change in E_{xx}. In order to obtain and observe the large stiffness changes due to transverse cracking needed to critically evaluate an analysis, specimens used in this investigation were fabricated from a glass-epoxy material system.

Four laminates, $[0,90_3]_s$, $[90_3,0]_s$, $[0,\pm45]_s$, and $[0,90]_s$ (type I,II,IV, and V materials, respectively), were investigated. One panel of each laminate was fabricated in-house from Scotchply Type 1003

reinforced plastic. Tension tests performed on $[0_4]$ and $[90_4]$ specimens and a rail shear test performed on $[0,90]_s$ material provided the lamina properties shown in Table 1. Three test sequences were used to evaluate the response of each laminate. In the first sequence, the longitudinal stiffness E_{xx} was monitored throughout the development of damage. In the second sequence, four stiffness components (E_{xx}, ν_{xy}, G_{xy}, and D_{yy}) were measured in the undamaged and near-saturation damage states. In the third test sequence, both the longitudinal stiffness (E_{xx}) and Poisson's ratio (ν_{xy}) were measured with two clip gages during damage development.

3.2 Longitudinal Stiffness Degradation Tests

3.2.1 Specimen Preparation

Tensile coupons 1.0 in. wide were cut from plates of each material. Specimens cut from the Type I panel were 7.9 in. long, while specimens cut for the other panels were 8.0 in. long.

Prior to testing, each specimen was polished in order to enhance the quality of edge replicas, which were made during the mechanical test. Initial work indicated that the edges of specimens cut with a diamond saw were at least as smooth as a surface polished with 600 grit emery paper, so specimens were polished with 5.0 micron and 3.0 micron alumina powder. A felt polishing cloth was wetted thoroughly with water and stretched over a flat surface. Alumina powder was then smeared into the wet polishing cloth. The specimen edge was repeatedly stroked lengthwise over the alumina-impregnated felt until the edge was polished to the desired surface finish. Usually fifty strokes was sufficient. Residual alumina slurry was rinsed from the specimen.

Next, the front specimen surface was washed with acetone. A center line was drawn along the length of the specimens on the clean surface. Two reference lines were drawn perpendicular to the center line so that they were 2.0 in. apart and equidistant about the midpoint of the centerline. Two-part epoxy adhesive was applied to the specimen surface to produce two thin strips of epoxy which spanned the specimen width along the reference lines. The epoxy strips were about 1/4 in. wide. The epoxy was allowed to cure at room temperature for 24 hours.

After the epoxy had cured, a straight razor was used to cut a groove perpendicular to the specimen centerline in the epoxy strip closer to that end of the specimen which would be inserted into the top grip of the testing machine. After this top groove was cut, the top knife edge of the 2.00 in. clip-on type extensometer was seated in the groove, and pressure was applied to the bottom knife edge of the extensometer so that it would leave an impression in the bottom epoxy strip. A groove was then cut along the impression left by the knife edge in the lower epoxy strip. These grooves constituted a seat for the clip gage during mechanical testing. It was important to cut the clip gage grooves in the epoxy tabs while the epoxy was still soft. If the epoxy was allowed to cure for several days, it became quite hard. It was then difficult to create an impression of the lower knife edge in the epoxy strip. In addition, the fatigue response of the epoxy seems to deteriorate with increasing cure time.

3.2.2 Mechanical Testing

The tensile coupons were loaded in uniaxial tension in a 20 kip servohydraulic MTS testing machine. Most specimens were subjected to quasi-static tensile loads in a load controlled testing mode. In such a loading sequence, the specimen was subjected to several loading-unloading ramps which sequentially increased in amplitude. The ramp rates used were 11.1 lbs/sec (22.2 lbs/sec for Type IV specimens) during loading and 20.0 lbs/sec (40.0 lbs/sec for Type IV specimens) during unloading. Longitudinal strain data was gathered during the ramp loading with a 2.00 in. gage lens clip-on type extensometer. A

permanent record of longitudinal strain versus load was generated with an x-y plotter.

In order to monitor the development of damage during the load history, an edge replication technique developed by Stalnaker and Stinchcomb [16] was used to record the damage at the specimen edge during each loading ramp. Caution was exercised so that the extensometer was not disturbed during the replication process. A 1.0 in. long strip of cellulose acetate was attached to the specimen edge within the gage section with transparent adhesive tape. A syringe was used to inject acetone between the acetate tape and the specimen edge. The acetone softened acetate was then pressed against the specimen edge. When the cellulose acetate hardened, it provided an impression of the edge surface which became a permanent record of the damage present at the specimen edge. Previously, standard replication procedure had been to maintain the maximum load of a given loading ramp while making a replica. However, in the case of the $[0,90_3]_s$ and $[90_3,0]_s$ laminates, a significant amount of damage developed while holding at moderate load levels. In order to limit the amount of damage that developed in any one quasi-static cycle, replicas were made while holding at 400 lb. on the unloading side of the ramp for those specimens.

An examination of edge replicas obtained during quasi-static tests performed on $[0,90]_s$ and $[0,\pm45]_s$ specimens revealed that even if replicas were made while holding at the maximum load of a quasi-static cycle, transverse cracks were not easily discernable. The crack opening was small, so the softened acetate tape did not readily flow into the

transverse cracks when replicas were made. Since the transverse cracks were not very distinct, it was difficult to obtain reliable crack counts. Tension-tension fatigue loads were applied to some Type IV and Type V specimens, as fatigue induced cracks appeared more distinct on edge replicas. It is believed that this increased clarity is a result of surface wear that occurs at the crack surface, during fatigue loading. The fatigue tests were performed in load control on a 20 kip servo-hydraulic MTS machine at a frequency of 10 Hz and a stress ratio of $R = 0.1$. Again, longitudinal strain was monitored with a 2.00 in. clip gage. Fatigue cycling was interrupted periodically in order to record longitudinal strain versus quasi-static load data and to obtain edge replicas.

3.3 Tensor Stiffness Evaluation

3.3.1 Specimen Preparation

In this testing sequence, four laminate stiffness components, E_{xx}, ν_{xy}, G_{xy}, and D_{yy}, were measured in the undamaged and near-saturation damage states. In order to accomodate the rail shear and bend test fixtures used to measure G_{xy} and D_{yy}, respectively, 2.00 in. wide coupons were cut from panels of each laminate. Type I coupons were 7.9 in. long while specimens from the other material types were 10.0 in. long.

Both specimen surfaces were cleaned thoroughly with acetone. Longitudinal and transverse reference marks were drawn on both surfaces of each specimen. Each specimen was instrumented with a 0,90,45 degree stacked strain rosette on the front surface.

3.3.2 The Bend Test

While some measure of the effect of transverse cracks on the transverse stress σ_{yy} in the damaged plies was desired, the specimen geometry was not well suited to a direct measurement of E_{yy}. Therefore, a bend test developed at VPI&SU by O'Brien [4] was used to measure the bending stiffness component D_{yy}. The bend test fixture provided two knife edges 1.75 in. apart which supported the specimen along its length. The specimen was loaded along the centerline of its back surface by the corner of a wedge that was 8.0 in. long. A schematic diagram of the testing configuration is shown in Fig. 7. The test fixture-specimen assembly sat atop a compressive load cell. The wedge was lowered onto the specimen at a constant crosshead rate of 0.005 in/min. When the

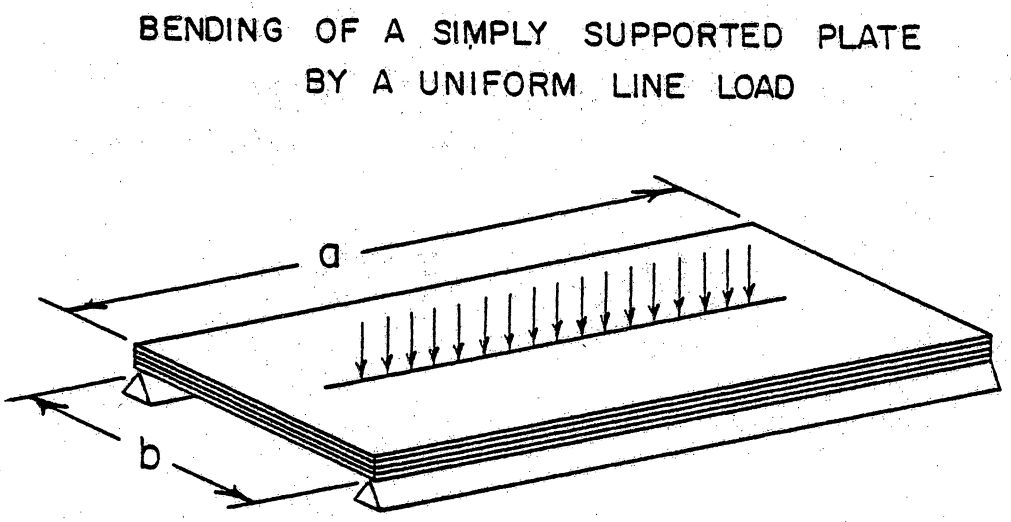

Fig. 7 Schematic diagram of the bend test configuration.

load cell registered a small compressive load, the crosshead was stopped and a magnetic base dial gage which was used to obtain an accurate measurement of crosshead (and specimen) displacement was zeroed. The load corresponding to this zero displacement was recorded. Crosshead travel was then continued, and load readings were taken when the dial gage indicated that the subsequent crosshead motion was 0.010 in., 0.015 in., and 0.020 in. This test procedure, including alignment of the test assembly under the loading wedge and positioning of the dial gage, was performed three times. The analytical series solution for a plate of infinite length, simply supported along its length, was used to obtain the bending stiffness D_{yy} from load-deflection data. Load cell deflection was neglected [5]. While load cell deflection did affect the measured bending stiffness, it was not expected to significantly affect measured changes in bending stiffness.

Bend test results are sensitive to specimen curvature. For example, in this investigation, one of the $[0,90_3]_s$ specimens was initially warped. Its initial bending stiffness was relatively low. When the specimen was damaged, the warpage was eliminated, and the bending stiffness was increased from that measured in the undamaged state. Generally, the bend test provided qualitative information about the change in bending stiffness with damage development.

3.3.3 The Rail Shear Test

A rail shear test developed at VPI&SU by O'Brien [4] was used to measure the shear stiffness G_{xy}. The rail shear fixture, shown in Fig. 8, is similar to that used in a more standard test. The difference

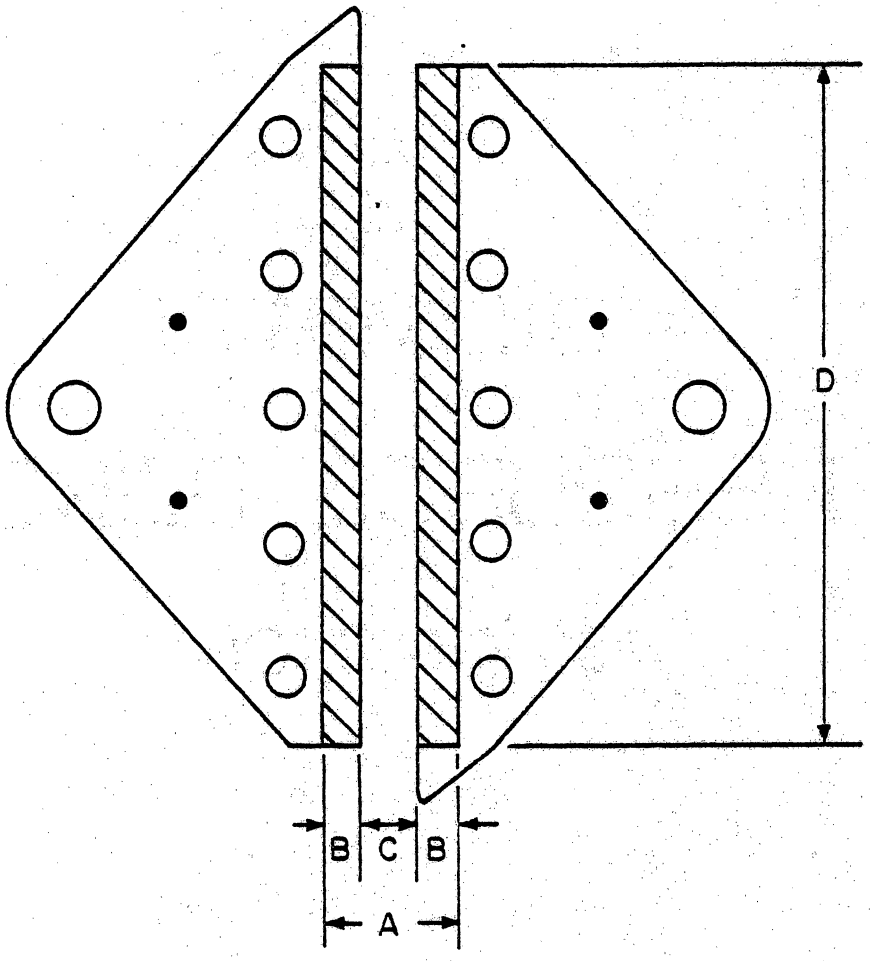

TABLE OF DIMENSIONS

	in	mm
A	2.000	50.80
B	0.625	15.88
C	0.750	19.05
D	10.0	254

Fig. 8 Schematic diagram of the rail shear apparatus.

is that this assembly grips the specimen only through friction forces, where the more common assembly has bolts that pass through holes drilled in the specimen. The absence of holes in the specimen insures a more uniform stress field in the specimen when other stiffness components are determined.

The specimens were carefully aligned in the rail shear loading fixture. They were placed in the fixture and maneuvered so that the two halves of the loading fixture were 0.75 in. apart and the longitudinal reference mark was equidistant for the edges of the two sides of the fixture. The transverse reference mark was aligned with the center tic marks scribed on the top plates of the rail shear rig. The bolts were first tightened finger tight, and then tightened with a torque wrench to 15 ft-lbs torque.

The rail shear tests were run on the 20 kip MTS machine in the load controlled testing mode. A compressive load ramp of 2 lbs/sec was used to shear the specimens. Specimens were loaded to 100 lbs. The shear strain ε_{45} was measured with the 45 deg gage of the strain rosette, and load versus shear strain was plotted with an x-y plotter. The outputs from the 0 deg and 90 deg gages were plotted against load on an X-Y-Y' plotter. The shear strain (γ_{xy}) is given by

$$\gamma_{xy} = 2\varepsilon_{45} - (\varepsilon_0+\varepsilon_{90}).$$

If a state of pure shear is attained, ε_0 and ε_{90} should vanish. At least two repetitions of the above loading process were performed on each specimen to insure consistency. Unless a given trial provided obviously discrepant data, trial averages were reported.

Because the rail shear test uses essentially a point strain measurement, the value of shear stiffness obtained for the damaged state is sensitive to the local details of the deformation field. The relative location of the strain rosette with respect to individual damage sites will affect the calculated value of shear stiffness. Therefore, this rail shear test provides only qualitative information about the shear stiffness of a damaged laminate.

3.3.4 Axial Loading Sequence

After initial bend and rail shear tests were performed, specimens were loaded in axial tension on the MTS machine described earlier. Specimens were subjected to ramp loadings at a ramp rate of 22.2 lbs/sec. Load and transverse strain (ε_{90}) were plotted against longitudinal strain (ε_0) on an X-Y-Y' recorder. Thus, longitudinal stiffness E_{xx} and Poisson's ratio ν_{xy} could be measured during each ramp loading. Specimens were subjected to load ramps that increased sequentially in amplitude until the longitudinal stiffness changed by an amount that indicated that the specimen was nearing CDS. At this point, axial loading was stopped, and bend and rail shear tests were performed on the now damaged specimens.

Again, because essentially point strain values were measured, results were subject to considerable variation due to the local details of the deformation field. The proximity of individual damage events affected the measurements. In some cases, the strain rosette actually failed because of the local severity of the strain field.

3.4 Two Component Global Stiffness Evaluation

3.4.1 Specimen Preparation

As indicated in the previous section, whenever a point strain measurement is made, the measured strain value depends on the local details of the deformation field. The location of the strain measurement with respect to individual damage events significantly affects the measured strain value. It is difficult to determine whether or not such a measurement provides a strain value indicative of global laminate response. On the other hand, a clip gage provides a measure of average strain over a relatively large gage length. Thus, a clip gage provides a measure of global strain that is less sensitive to the local details of the damage state. A test was developed in which longitudinal and transverse strain were measured simultaneously with clip gages during load application.

Specimens 2.0 in. wide and 10.0 in. long were cut from the type II,IV, and V laminates. Because of a shortage of material no type I specimens were tested. Two transverse strips of two-part epoxy adhesive were applied to the front specimen surface 2.0 in. apart and equidistant from the transverse centerline of the specimen. Transverse grooves were cut in the epoxy strips to accomodate the knife edges of a 2.0 in. gage length clip-on type extensometer as described in Section 3.2.1. Two 1.0 in. long longitudinal strips of epoxy adhesive were applied to the back surface 1.0 in. apart and equidistant from the longitudinal centerline of the specimen. Longitudinal grooves were cut in these epoxy strips to accomodate the knife edges of a 1.0 gage length clip gage that

was used to measure transverse strain. During testing, the clip gages were held in place with rubber bands. A schematic diagram illustrating the assembly of the extensometers and specimen is shown in Fig. 9.

3.4.2 Mechanical Testing

The 20 kip MTS machine was used to load the specimens in simple tension. Each specimen was subjected to a series of ramp loadings (ramp rates: 22.2 lbs/sec on loading, 40 lbs/sec on unloading) that increased sequentially in amplitude. Longitudinal and transverse strain were measured with the 2.0 in. gage length clip gage on the front surface and the 1.0 in. gage length clip gage on the back surface, respectively. Load and transverse strain were plotted against longitudinal strain on an X-Y-Y' recorder during each load cycle.

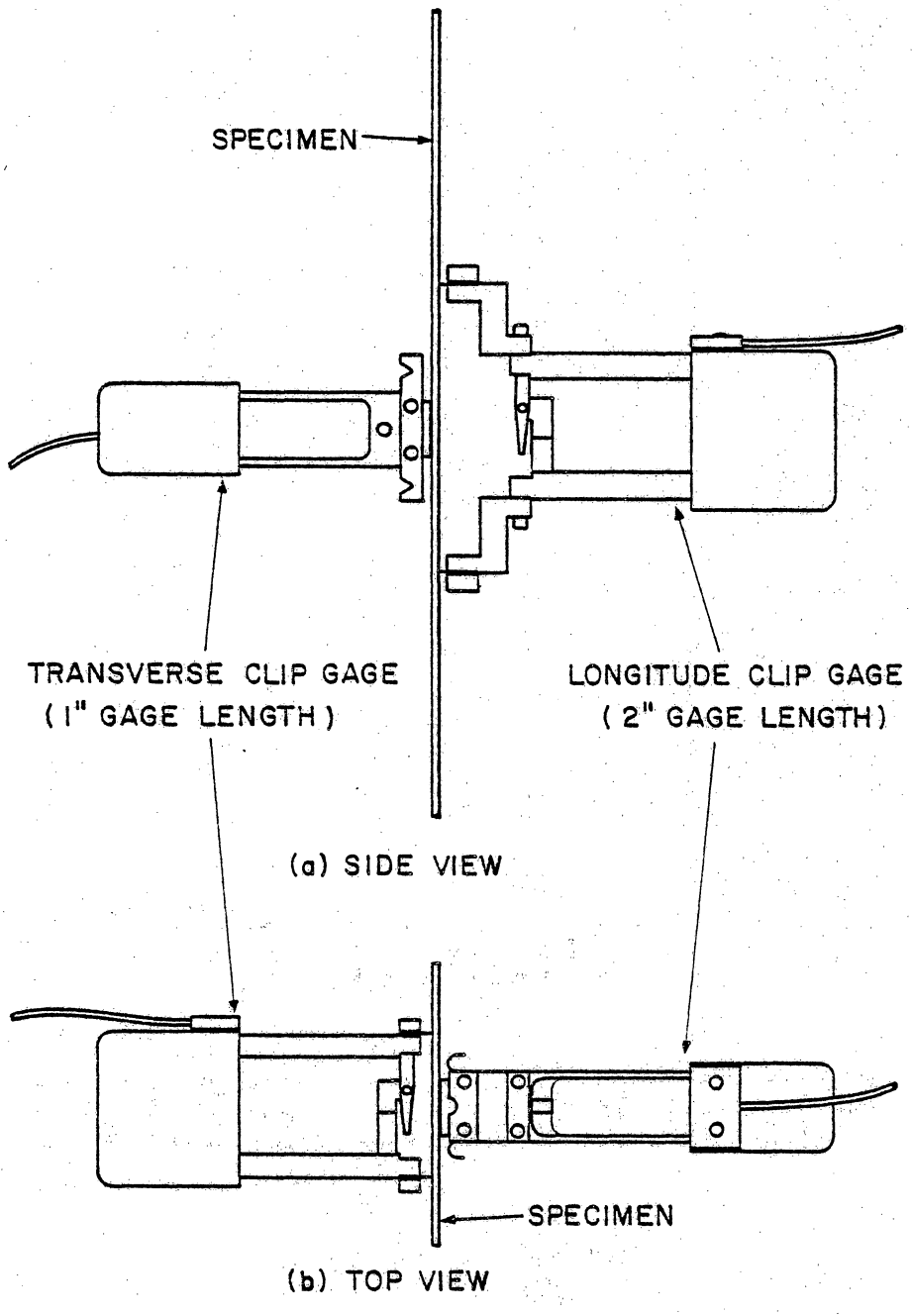

Fig. 9 Clip gage configuration for Poisson's ratio measurement.

IV. RESULTS AND DISCUSSION

4.1 Lamina Stiffness Evaluation

Lamina stiffnesses of the glass-epoxy material system used were determined from axial stress versus strain measurements performed on $[0_4]$ and $[90_4]$ specimens, and a rail shear test performed on a $[0,90]_s$ specimen. The resulting lamina properties are shown in Table 2. These properties were used as input data for the shear lag model and the modified laminate analysis. However, panel-to-panel variations in laminate properties precluded the use of the analyses to predict actual laminate stiffnesses. For example, undamaged type I specimens had a longitudinal stiffness of about 3.05 Msi, while undamaged type II specimens had a longitudinal stiffness of about 2.50 Msi. Laminate analysis indicates that these two laminates should have the same longitudinal stiffness. Therefore, predicted stiffnesses were normalized with respect to the predicted stiffness of the undamaged laminate, and compared to normalized observed stiffnesses.

4.2 $[0,90_3]_s$ Laminates

The $[0,90_3]_s$ laminates were expected to exhibit large stiffness changes after transverse cracking occurred. Typical longitudinal stiffness evaluation data for a $[0,90_3]_s$ specimen, in this case specimen A2, is shown in Fig. 10. The initial stiffness was approximately 3.0 Msi. The general trend indicated by the plot is that as the crack density increased, the stiffness decreased. At the higher load levels, both the stiffness and the crack density reached relatively stable values; the

Table 2. Material properties for glass-epoxy (V_f = 0.63).

Material	E_1 (Msi)	E_2 (Msi)	ν_{12}	G_{12} (Msi)	Ply Thickness (in.)
E-Glass	6.05	1.89	0.300	0.63	0.008

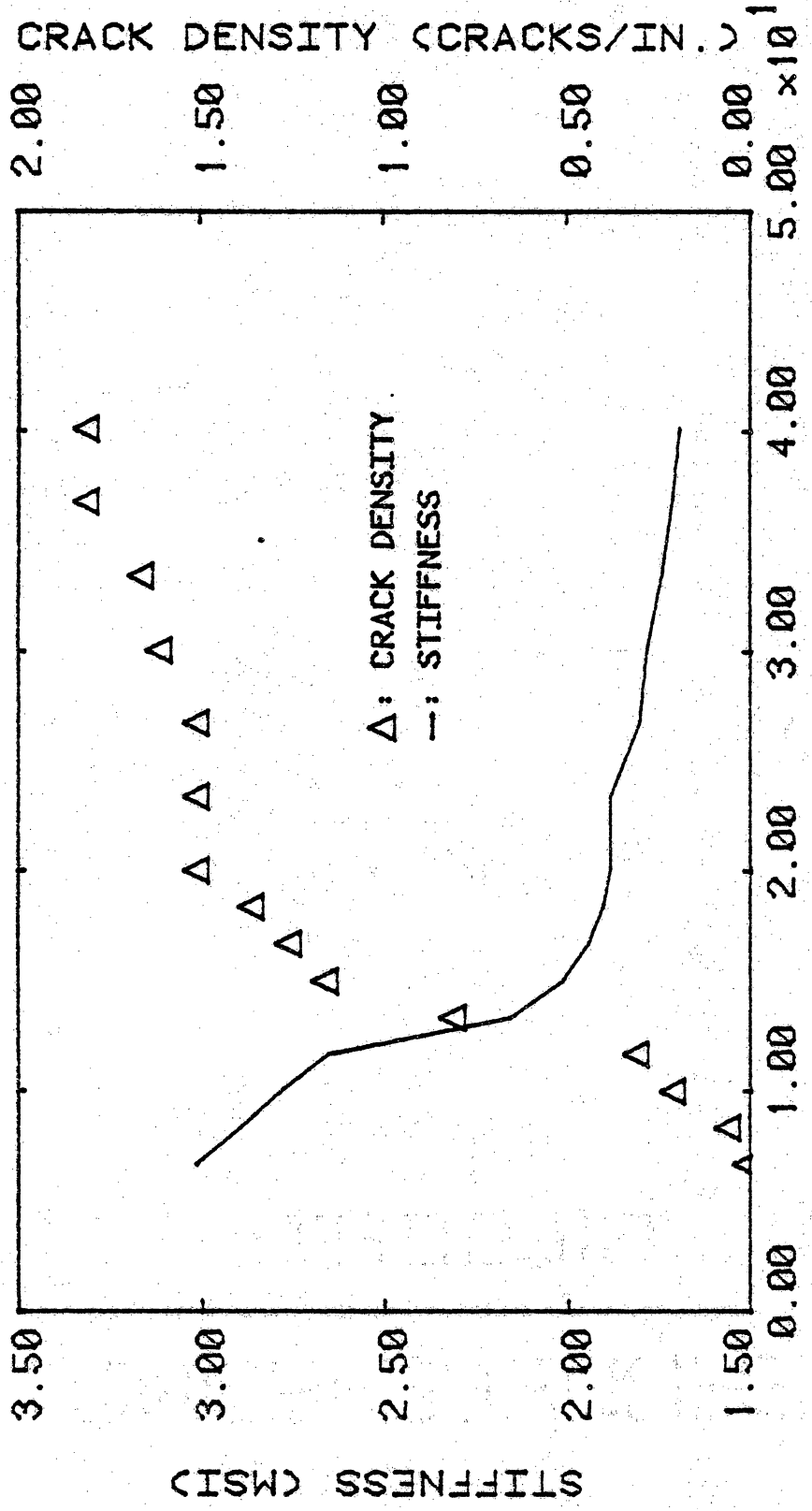

Fig. 10 Stiffness and crack density versus stress level for specimen A2.

maximum crack density was about 18 cracks/in., and the minimum stiffness was about 1.6 Msi. The stable crack density indicated that the CDS for this laminate had been attained. Figure 11 shows that large increases in crack density occurred simultaneously with large decreases in stiffness; when smaller increases in crack density occurred, the stiffness decrease was also smaller. Good correlation between stiffness and crack density was indicated, and the stiffness change, which was expected to be large, was 45 percent.

A portion of the edge replica history of specimen A2 is presented in Fig. 12. At low applied stress levels (Fig. 12a) little or no transverse cracking was observed in the edge replicas. Note that there was no apparent resin-rich region between adjacent 90 deg plies in the interior of the laminate. After the application of a moderate applied stress (Fig. 12b), the majority of the transverse cracks had developed. These cracks crossed all of the 90 deg plies and extended to very near the 0,90 interface. If the edge replicas were observed under a high magnification (400x), numerous tiny matrix cracks dispersed through the medium were seen. The matrix cracks of interest here were only those that crossed an entire ply or set of plies, and thus constituted a significant structural defect within the composite laminate. At high applied stress levels (Fig. 12c), the transverse cracks attained a nearly uniform spacing and further application of load did not significantly affect the crack density. In addition, crack branching, smaller cracks extending from larger ones, was seen.

The shear lag model was used to predict longitudinal stiffness as a function of crack density. In the analysis, crack spacing was assumed

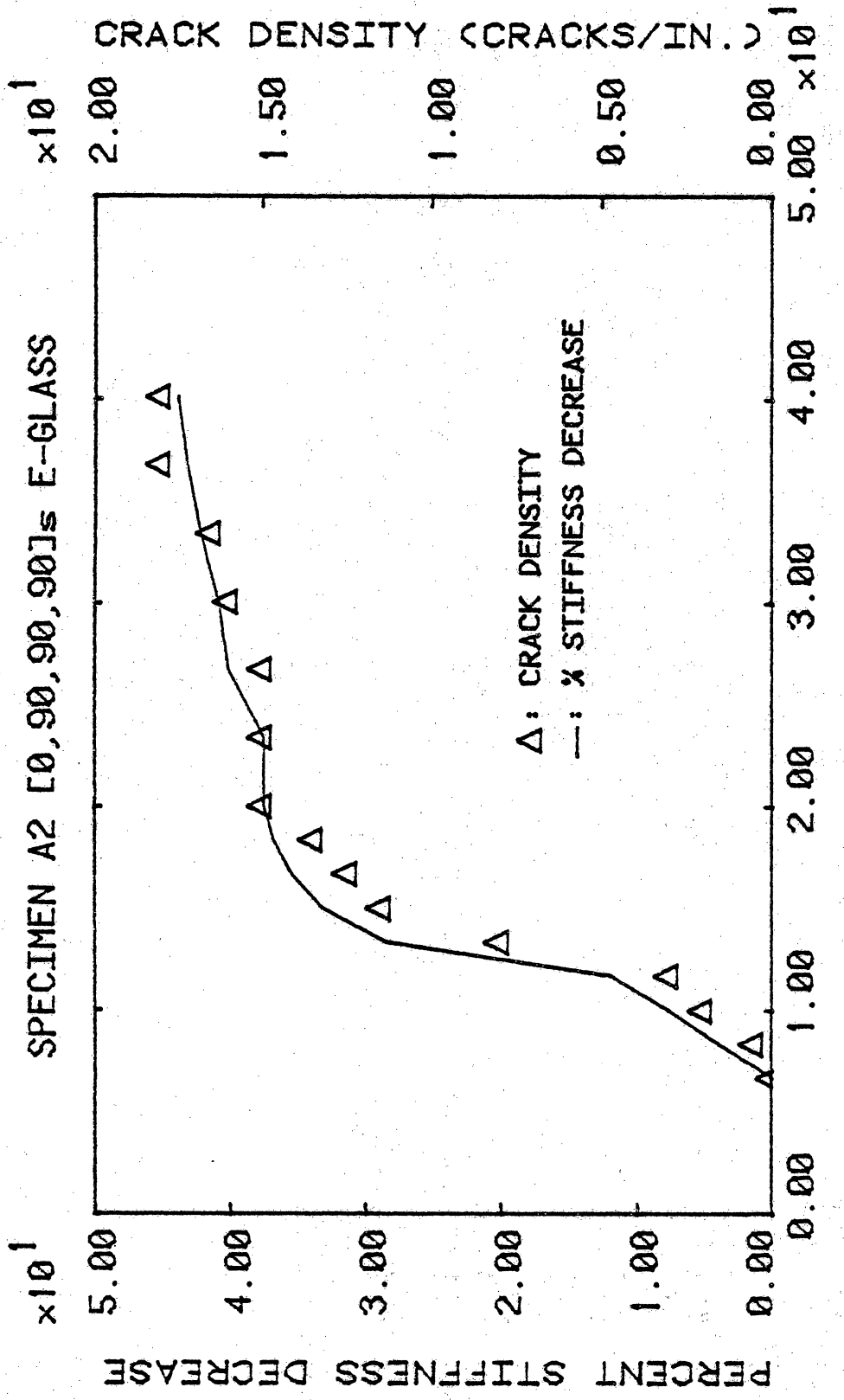

Fig. 11 Stiffness decrease and crack density vs. stress level for specimen A2.

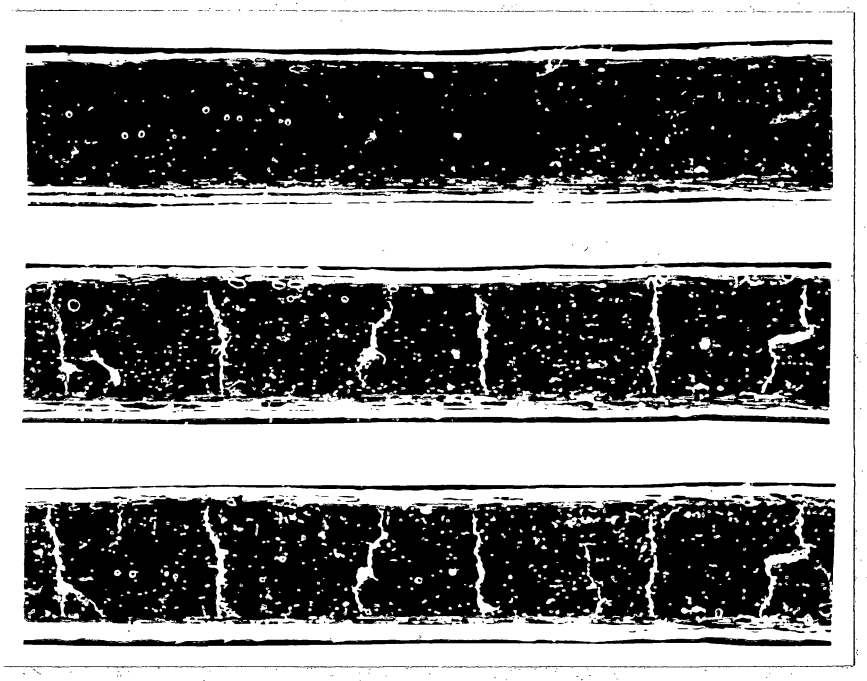

Fig. 12 Partial edge replica history of specimen A2.

to be uniform throughout damage development. Usually, the spacing was only uniform at the CDS. In Fig. 13, theoretical predictions and experimental observations for normalized stiffness as a function of crack density are shown. A comparison of the shear lag predictions with experimental results indicated that while the general shape of the predicted curve is correct, the stiffness was overestimated. Some difference between theory and experiment was expected since damage was not restricted to exclusively transverse cracking. As shown, the shear lag analysis predicted a 40 percent stiffness reduction, while a reduction of 45 percent was observed. The dashed line indicates the axial stiffness predicted by a laminate analysis in which E_2 of the 90 deg plies had been reduced to zero. Of importance was that this prediction and the shear lag prediction bounded the observed results. Also, the laminate analysis provided a reasonable, and for design considerations, conservative estimate for the longitudinal stiffness when damage was fully developed.

Results from the tensor stiffness evaluation of the $[0,90_3]_s$ material are shown in Table 3. Because of experimental difficulties, the tabulated values were not all obtained from the same specimen. Longitudinal stiffness and Poisson's ratio were obtained from quasi-static test data for a 1.0 in. wide tensile coupon (specimen A5) that was instrumented with a biaxial strain rosette. Shear modulus data was obtained from specimen A9. The original strain gage malfunctioned during quasi-static loading to induce damage, so the specimen was re-instrumented in order to obtain a shear modulus for the damaged material. The bridge amplifier gains were different for the two measurements, so

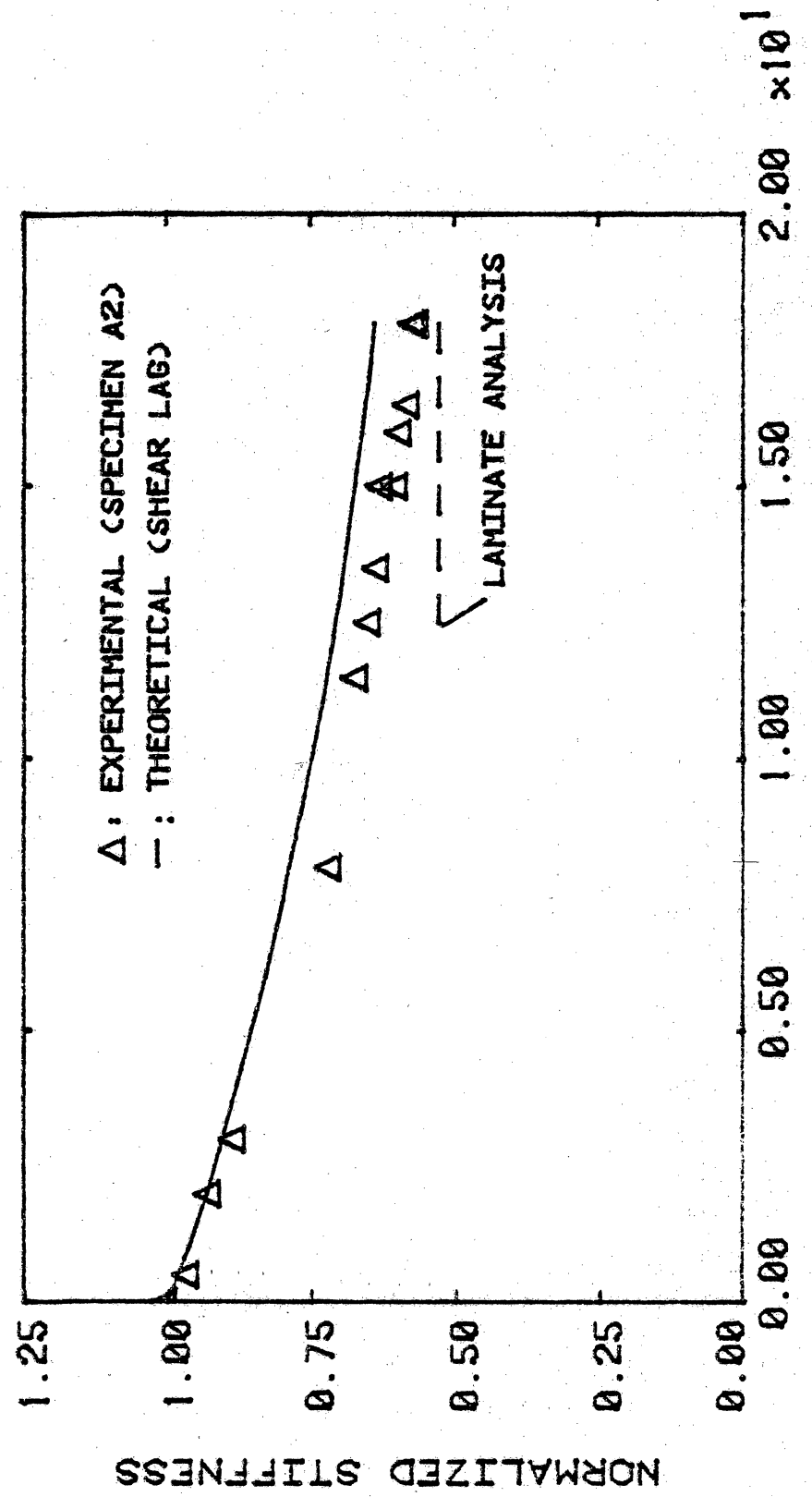

Fig. 13 Predictions and measurements of stiffness as a function of crack density for a $[0,90_3]_s$ laminate.

Table 3. Results of tensor stiffness evaluation of type I material.

Property	Undamaged State Evaluation	Damaged State Evaluation	% Reduction (Observed)	% Reduction (Predicted)
E_{xx}	2.92 Msi	1.98 Msi	32.2	47.8
ν_{xy}	0.13	0.06	54.0	74.3
G_{xy}	0.97 Msi	0.93 Msi	3.9	0.0
D_{yy}	4.50 ksi-in.^{2}	4.48 ksi-in.^{2}	0.6	3.4

the shear modulus data was, at best, qualitative. The bending stiffness of the undamaged material was determined from specimen B9, while the bending stiffness of the damaged material was determined from specimen A9. Of particular interest was Poisson's ratio, which decreased by 54 percent during damage development. The shear moduli and bending stiffnesses shown were approximate, but did indicate that changes in these stiffnesses were small compared to changes in E_{xx} and ν_{xy}. Also shown in Table 3 are stiffness decreases predicted by a modified laminate analysis. Correlation between predicted and observed stiffness reductions was reasonable.

4.3 $[90_3,0]_s$ Laminates

As with the type I material, the $[90_3,0]_s$ laminates were expected to exhibit large stiffness changes after transverse cracking occurred. The in-plane stiffnesses predicted by laminate analysis and the shear lag analysis were identical for the type I and type II laminates. Figure 14 illustrates typical quasi-static test results for a $[90_3,0]_s$ specimen, in this case specimen II-1. The results were similar to those for the $[0,90_3]_s$ laminate in that the stiffness decrease was large (37%), and that when the crack density increased, the stiffness decreased. The crack density did not quite reach a stable value at high stress levels. The significant differences were that both the initial stiffness (2.50 Msi) and the final crack density (14 cracks/in.) were lower than the corresponding values for the $[0,90_3]_s$ laminates.

A portion of the edge replica history of specimen II-1 is presented in Fig. 15. The trends seen were similar to those cited for the type I

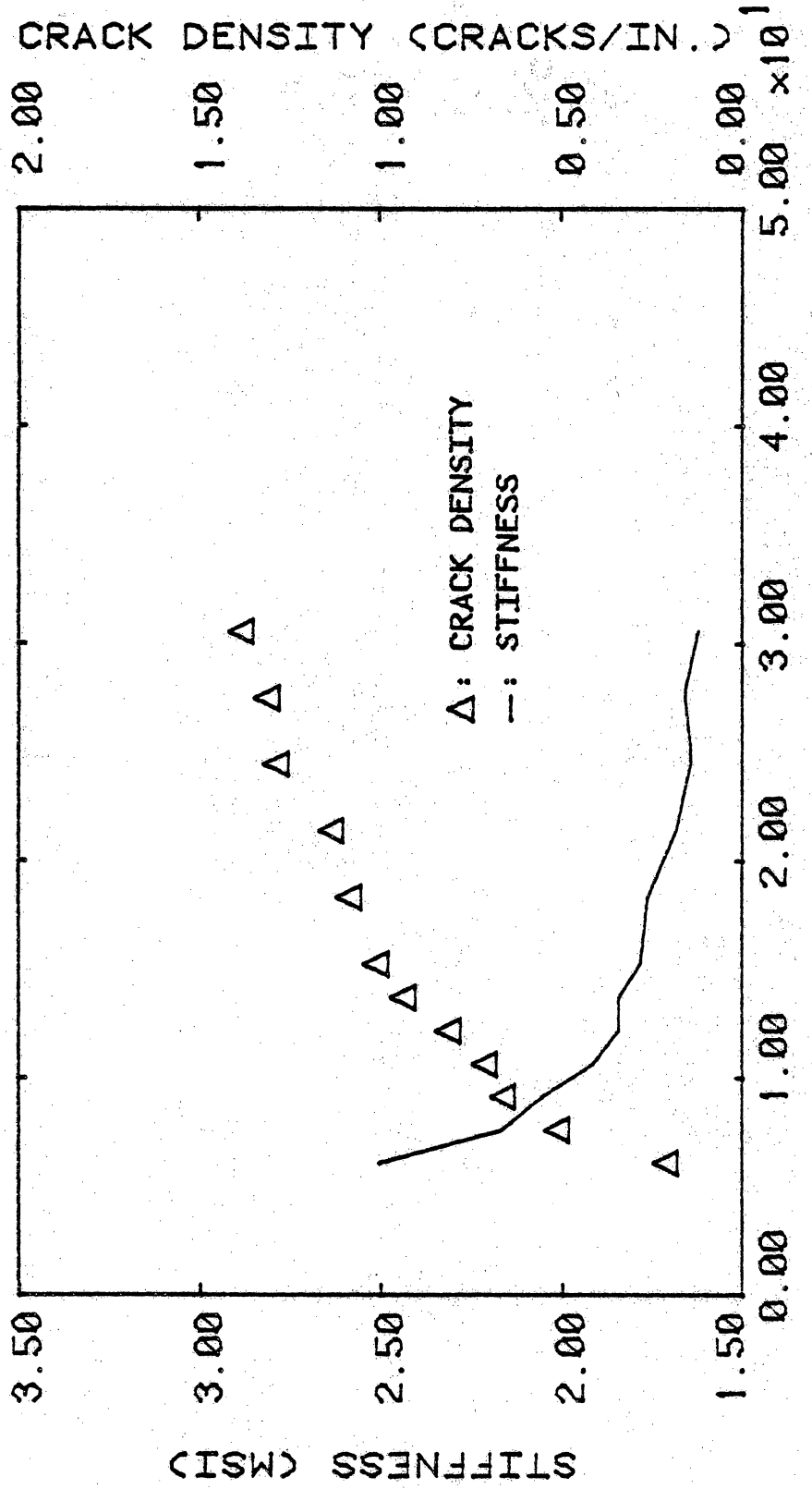

Fig. 14 Stiffness and crack density vs. stress level for specimen II-1.

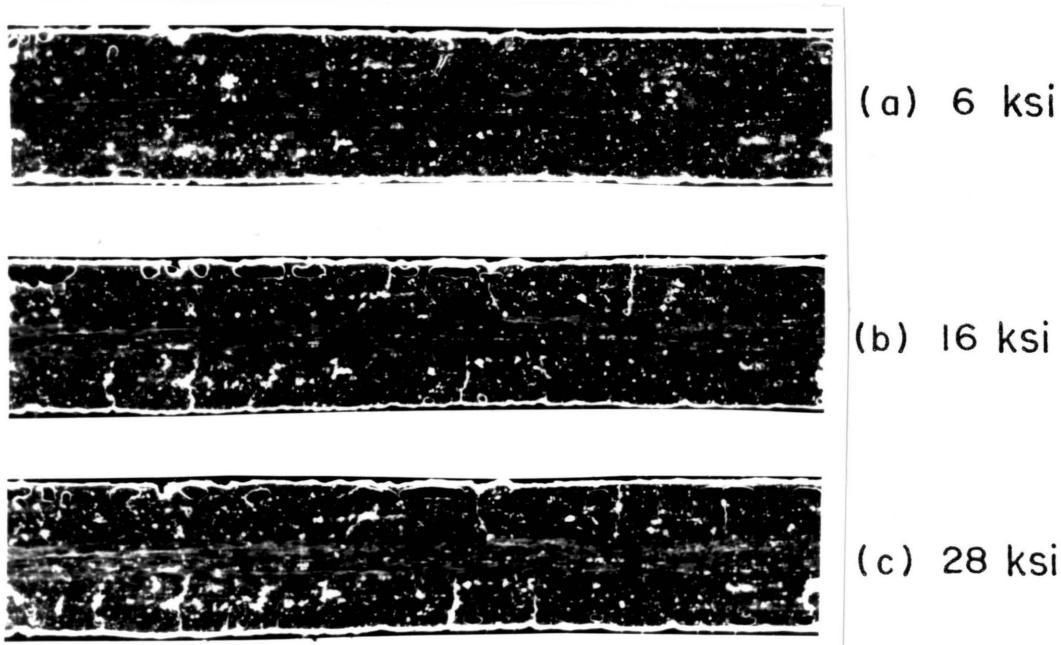

Fig. 15 Partial edge replica history of specimen II-1.

material. Initially (Fig. 15a), few transverse cracks were observed. After an average stress of about 15 ksi had been applied, most of the cracks that would form had formed. Eventually, a nearly uniform crack spacing was attained at high stress levels (Fig. 15c). Some crack branching was observed near the 0,90 interface.

In Fig. 16, theoretical predictions and experimental observations of normalized stiffness as a function of crack density are shown. Again the shear lag model correlated well with experiment, and the model overestimated the stiffness of the laminate at severe damage states. The modified laminate analysis underestimated the laminate stiffness, and the shear lag and laminate analysis predictions bounded the observed results.

Results from the tensor stiffness evaluation of the $[90_3,0]_s$ material are shown in Table 4. The changes in longitudinal modulus and Poisson's ratio during damage development were large, while the shear stiffness and bending stiffness did not change appreciably. Correlation of modified laminate analysis predictions with observed results was good.

Global stiffness measurements were made for specimen II-10 using the two clip gage technique. In the undamaged state, the measured values of longitudinal stiffness and Poisson's ratio were E_{xx} = 2.85 Msi and ν_{xy} = 0.103. In the near-saturation damage state they were E_{xx} = 1.74 Msi and ν_{xy} = 0.03. The corresponding stiffness changes, a 39 percent decrease in E_{xx} and a 71 percent decrease in ν_{xy}, correlated well with predictions from the modified laminate analysis.

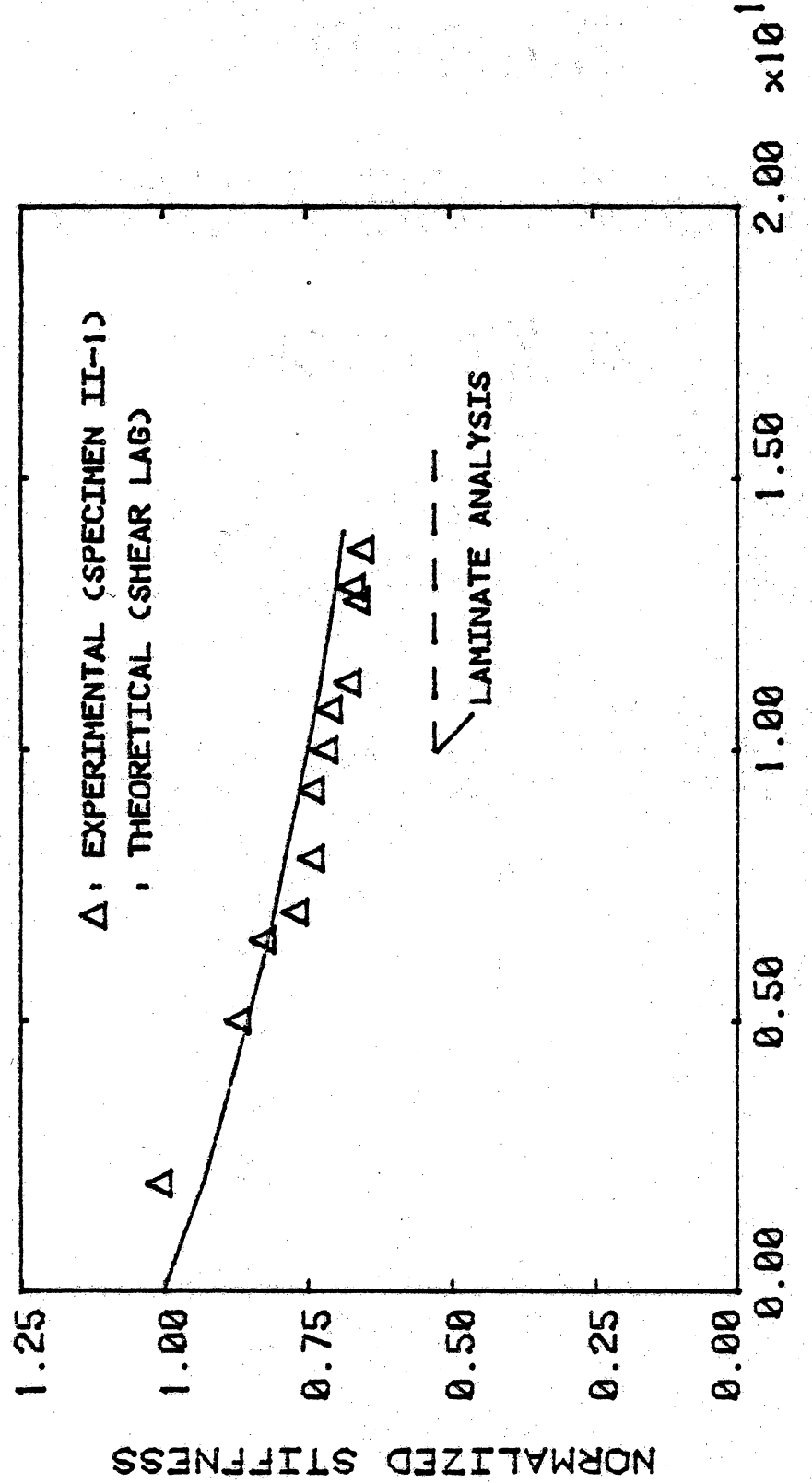

Fig. 16 Predictions and measurements of stiffness as a function of crack density for a $[90_3,0]_s$ laminate.

Table 4. Results of tensor stiffness evaluation of type II material (specimen II-9).

Property	Undamaged State Evaluation	Damaged State Evaluation	% Reduction (Observed)	% Reduction (Predicted)
E_{xx}	2.73 Msi	1.81 Msi	33.7	47.8
ν_{xy}	0.136	0.047	65.0	74.3
G_{xy}	0.71 Msi	0.71 Msi	0.0	0.0
D_{yy}	7.31 ksi-in.^{2}	7.33 ksi-in.^{2}	- 0.3	2.0

4.4 $[0,90]_s$ Laminates

Fatigue results for $[0,90]_s$ specimen V-6 are shown in Fig. 17. The maximum stress applied during each fatigue cycle was 30 ksi ($\sigma_{max} = 0.5\ \sigma_{ult}$). The initial stiffness was 3.29 Msi, and decreased to 2.93 Msi within the first 10,000 fatigue cycles. The stiffness decreased more slowly over the next 90,000 cycles to a stable value of about 2.80 Msi. The total stiffness decrease was about 15 percent. During the first 10,000 cycles, the crack density increased from a near zero value, to about 40 cracks/in. During the final 90,000 cycles, the change in crack density was small; the crack density reached a stable value of 49 cracks/in. Again, a large increase in crack density was accompanied by a large decrease in stiffness. The shear lag model was not used to predict longitudinal stiffness degradation with increasing crack density because the imposition of boundary conditions resulted in a system of equations that was ill-conditioned, and could not be solved by the existing solution scheme.

An examination of the edge replica history of specimen V-6 revealed that after the first 1/2 cycle of loading, the crack density in the 90 deg plies was quite high (Fig. 18a). As seen in Fig. 18b, after 5,000 cycles of fatigue loading the spacing of the transverse cracks was nearly uniform. The further application of load cycles degraded the overall integrity of the laminate. Figure 18d shows that after 100,000 cycles, delaminations between the 90 deg plies had developed, and edge damage had developed in the 0 deg plies. These additional damage modes were, for the most part, limited to those specimens that were loaded cyclically.

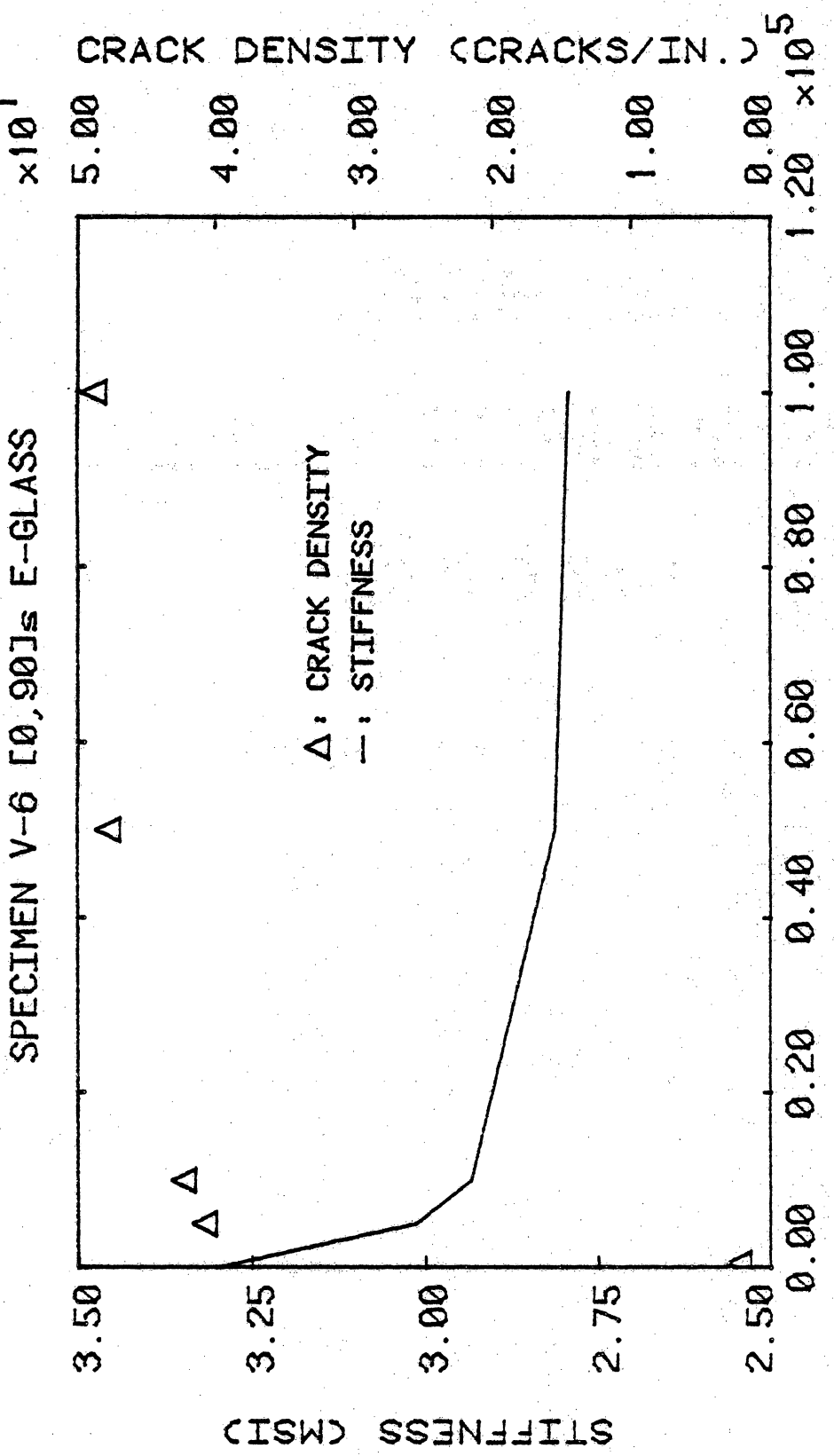

Fig. 17 Stiffness and crack density vs. cycles of loading for specimen V-6 ($\sigma_{max} = 0.50\ \sigma_{ult}$, R=0.1).

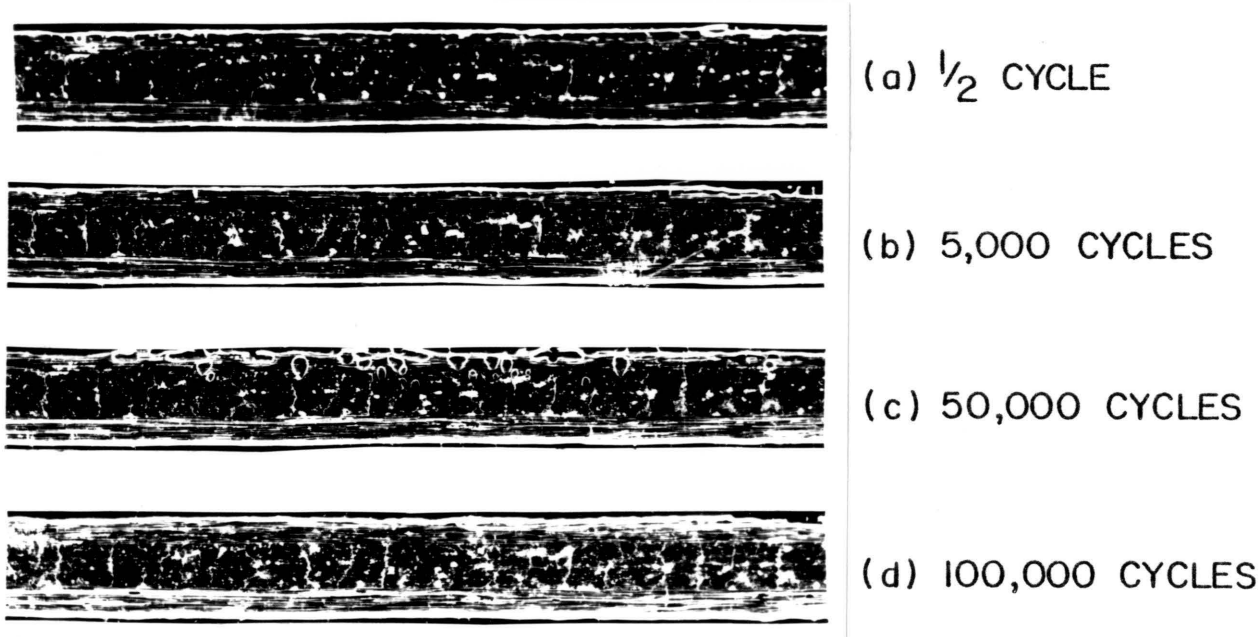

Fig. 18 Partial edge replica history of specimen V-6.

Results from the tensor stiffness evaluation of the type V material are shown in Table 5. Generally, the stiffness reduction data was in disagreement with the modified laminate analysis predictions. The only stiffness component that was in reasonable agreement with the theoretical prediction is the bending stiffness. This was the only stiffness value that was not determined from a strain gage measurement. A global laminate stiffness evaluation performed on specimen V-12 using the biaxial clip gage technique provided stiffness reduction data that was in close agreement with the modified laminate analysis predictions. The values of longitudinal stiffness and Poisson's ratio obtained in the undamaged state were E_{xx} = 3.93 Msi and ν_{xy} = 0.108. The stiffnesses measured in the damaged state were E_{xx} = 3.26 Msi and ν_{xy} = 0.047. These measurements indicated a 17.1 percent reduction in E_{xx} and a 49.8 percent reduction in ν_{xy}, which were in close agreement with the theoretical predictions. Note the discrepancy between the clip gage data and the strain gage data. Because the strain gage data was more sensitive to local disturbances in the deformation field, the strain gage data was suspect.

4.5 $[0,\pm45]_s$ Laminates

Fatigue data for specimen IV-9, a representative $[0,\pm45]_s$ laminate, is shown in Fig. 19. The maximum stress applied during the fatigue cycling was 25 ksi (σ_{max} = 0.5 σ_{ult}). The decrease in stiffness over the first 10,000 cycles was large, and beyond 10,000 cycles the stiffness change was small. Also, during the first 10,000 fatigue cycles virtually all of the cracking occurred in both the +45 deg and -45 deg

Table 5. Results of tensor stiffness evaluation of type V material (specimen V-9).

Property	Undamaged State Evaluation	Damaged State Evaluation	% Reduction (Observed)	% Reduction (Predicted)
E_{xx}	4.06 Msi	3.65 Msi	10.1	22.6
ν_{xy}	0.193	0.165	14.5	48.9
G_{xy}	0.63 Msi	0.56 Msi	11.2	0
D_{yy}	73.3 psi-in.^{2}	68.0 psi-in.^{2}	7.3	1.0

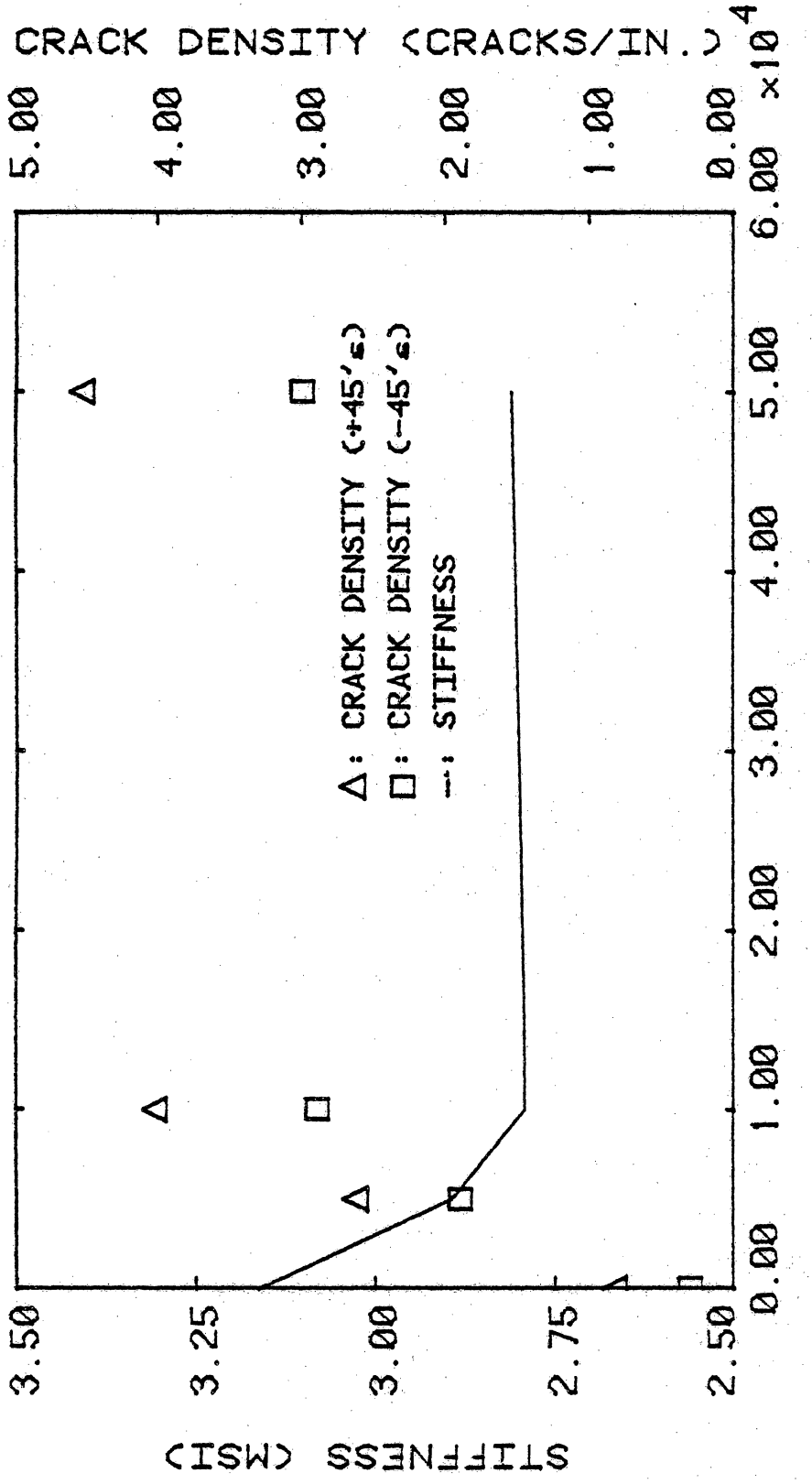

Fig. 19 Stiffness and crack density vs. cycles of loading for specimen IV-6 ($\sigma_{max} = 0.50\ \sigma_{ult}$, R=0.1).

plies, and after 10,000 cycles both of those crack densities had reached stable values. The stable crack density in the +45 deg plies was about 46 cracks/in., while the stable crack density in the -45 deg plies was about 30 cracks/in.

The damage states that developed in the type IV laminates were more complex than those that developed in the other laminates. The edge replica history of specimen IV-6 is shown in Fig. 20. Initially, few transverse cracks were detected in the edge replicas. After 5,000 cycles of fatigue loading, a few cracks were detected, and the cracks in the +45 deg plies were not very distinct. After 10,000 cycles, essentially uniform crack spacing was attained in both the +45 and -45 deg plies. Subsequent fatiguing to 50,000 cycles caused further degradation of the material. Both delamination along the +45,-45 interface and fiber breaks in the 0 deg plies were observed in the edge replicas. In addition, longitudinal matrix crazing had developed in the 0 deg plies.

Results from the tensor stiffness evaluation of the type IV material are shown in Table 6. The predicted and observed stiffness changes did not agree. The shear stiffness changed by 28.4 percent, which was the largest change in shear stiffness observed for any of the laminates. Stiffness reductions measured via the biaxial clip gage technique also disagreed with the predicted values. The two clip gage technique was used on specimen IV-13. In the undamaged state, the values obtained for longitudinal stiffness and Poisson's ratio were E_{xx} = 3.54 Msi and ν_{xy} = 0.525. In the near-saturation damage state they were E_{xx} = 3.21 Msi and ν_{xy} = 0.488. During the course of damage development,

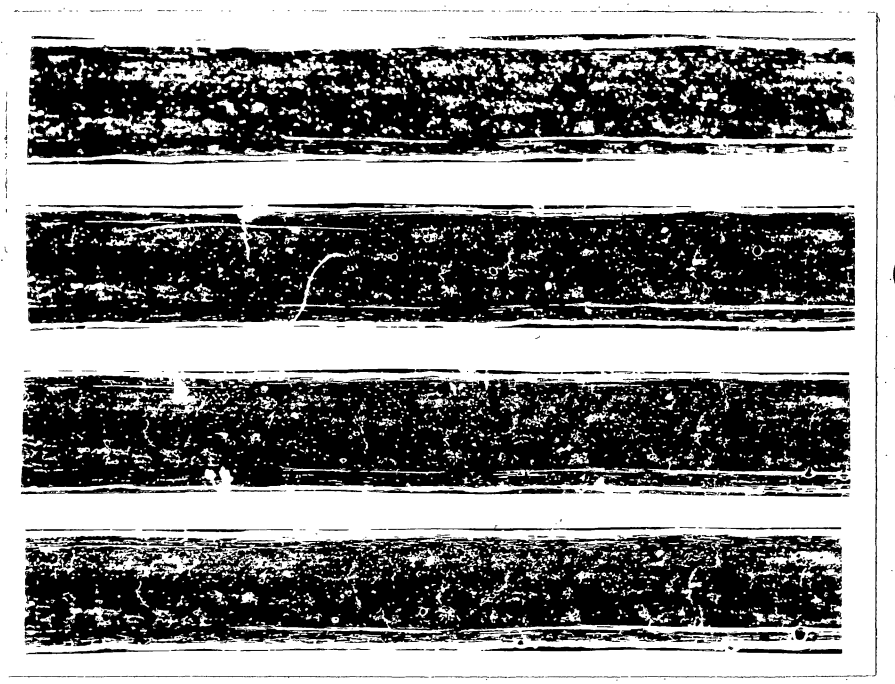

Fig. 20 Edge replica history of specimen IV-6.

Table 6. Results of tensor stiffness evaluation of type IV material (specimen IV-13).

Property	Undamaged State Evaluation	Damaged State Evaluation	% Reduction (Observed)	% Reduction (Predicted)
E_{xx}	3.57 Msi	3.25 Msi	9.0	4.7
ν_{xy}	0.476	0.465	2.3	25.6
G_{xy}	1.43 Msi	1.02 Msi	28.4	11.6
D_{yy}	0.218 ksi-in.^{2}	0.208 ksi-in.^{2}	5.3	10.6

the longitudinal stiffness decreased by 9.4 percent, while Poisson's ratio decreased by 8.1 percent. It was not surprising that the correlation between the analytical predictions and the experimental observations was not good for this material. For this laminate, damage was not restricted to transverse cracking. Three other damage modes--delamination, fiber breakage in the 0 deg plies, and longitudinal matrix crazing in the 0 deg plies--were observed. In addition, an earlier investigation of $[0,\pm45]_s$ boron-epoxy laminates found significant numbers of broken fibers in the +45 and -45 deg plies [17]. Such damage may have influenced the response of the $[0,\pm45]_s$ glass-epoxy material tested in this investigation. These additional damage modes were not accounted for in the modified laminate analysis used here.

4.6 Summary

The results for all four cases can be summarized in general terms. As the loading was increased, either in stress level for a quasi-static test or in number of cycles for a fatigue test, the crack density increased until it reached some stable value. During this process, the stiffness decreased and reached a stable value when the crack density did. Further, the rate of increase of the crack density was related to the rate of decrease of the stiffness. Large stiffness changes occurred when large crack density changes occurred, and small stiffness changes occurred when small crack density changes occurred.

A comparison of measured changes in the four stiffness components E_x, ν_{xy}, G_{xy}, and D_{yy} with corresponding laminate analysis predictions for all four stacking sequences is given in Table 7. For the $[0,90_3]_s$,

$[90,_3 0]_s$, and $[0,90]_s$ cases, the predicted values and measured values were in close agreement. Some longitudinal matrix crazing in fiber direction in the 0 deg plies, was observed and might account for the difference between the observed and predicted changes in D_{yy} in these cases. The measured change in G_{xy} for the $[0,90]_s$ material was not unreasonable because of the local nature of the strain measurement of a strain gage. In the $[0,90_3]_s$, $[90_3 0]_s$, and $[0,90]_s$ cases, the analysis was somewhat conservative; it overestimated the longitudinal stiffness change. Agreement between theory and experiment for the $[0,\pm 45]_s$ case was not good, but in this laminate, other damage modes were observed. Fiber breakage in the 0 deg plies, longitudinal splitting, and local delamination were all evident in the $[0,\pm 45]_s$ material, and thus could also be expected to contribute to the overall degradation of the mechanical response of the laminate. In addition, in a previous investigation of $[0,\pm 45]_s$ boron-epoxy laminates, a significant amount of fiber breakage was found in the +45 deg and -45 deg plies. The simple analysis postulated did not account for these additional damage modes.

Table 7. Predicted and observed stiffness decreases for glass-epoxy laminates.

Type	Material		ΔE_x (%)	$\Delta \nu_{xy}$ (%)	ΔG_{xy} (%)	ΔD_{yy} (%)
I	$[0,90_3]_s$	Observed	32.2*	54.0*	3.9	0.6
		Predicted	47.3	74.3	0.0	3.4
II	$[90_3,0]_s$	Observed	38.3	71.0	0.0	0.0
		Predicted	47.3	74.3	0.0	2.0
V	$[0,90]_s$	Observed	17.1	49.8	11.2	7.3
		Predicted	22.6	48.9	0.0	1.0
IV	$[0,\pm 45]_s$	Observed	9.4	8.1	28.4	5.3
		Predicted	4.7	25.6	11.6	10.6

*Obtained from strain gage data.

V. CONCLUSIONS

The objective of this investigation was to observe experimentally stiffness changes resulting from transverse cracking in off-axis plies and to model those changes analytically. Stiffness versus transverse cracking data was gathered for $[0,90_3]_s$, $[90_3,0]_s$, $[0,90]_s$, and $[0,\pm45]_s$ glass-epoxy laminates. Three models of varying complexity were evaluated.

Experimentally, large stiffness changes resulting from transverse cracking were measured, particularly in the $[0,90_3]_s$ and $[90_3,0]_s$ laminates. The $[0,90_3]_s$, $[90_3,0]_s$, and $[0,90]_s$ laminates developed damage states that were limited almost exclusively to transverse cracking. The damage state that developed in the $[0,\pm45]_s$ laminates was more complex, as, in addition to transverse cracking, delamination, fiber breakage in the 0 deg plies, and longitudinal matrix crazing in the 0 deg plies were observed. In addition, a general comment about stiffness measurement can be made. Since the deformation field in a damaged composite is inhomogeneous, when a laminate stiffness is to be determined after a severe damage state has developed in the laminate, a deformation measurement made over a larger test section better characterizes laminate response than a deformation measurement made over a smaller test section.

Of the analyses, the most sophisticated model, the finite difference model, proved least useful for predicting the response of a damaged laminate, because this model could solve only a few highly specialized problems. The shear lag model predicted changes in longitudinal stiffness with increasing transverse crack density that

correlated well with physical data for the $[0,90_3]_s$ and $[90_3,0]_s$ materials. The results from this investigation indicate that the shear lag analysis shows promise as a method for predicting the degradation of longitudinal stiffness during damage development for other laminates, provided an appropriate scheme for imposing end boundary conditions can be developed.

The proposed modified laminate analysis was able to predict reductions in longitudinal stiffness, Poisson's ratio, and bending stiffness that correlated well with experimentally observed reductions in these stiffnesses for the type I,II, and V laminates at near-saturation damage states. The shear modulus results for these materials, which indicate that relatively small changes in shear modulus occur due to transverse cracking, are inconclusive. If strain rosette failure during damage introduction (which occurred in about one half of the attempts at tensor stiffness evaluation) results from the rosette being located in a region where the strain is severe, then a rosette that survives damage introduction is located in a relatively mild region of the strain field. Strains measured in such a region may not accurately characterize laminate response. The stiffness degradation of the type IV laminates, laminates that exhibited damage modes other than transverse cracking, was not modeled well by the simple laminate analysis that accounted for only transverse cracking. This indicates that a comparison of measured tensor stiffness reduction with those predicted by this simple analysis may serve to characterize the damage state in a laminate where direct observations of damage in the laminate are not made. The results of

this investigation indicate that a modified laminate analysis (not necessarily the one postulated here) is capable of predicting tensor stiffness reductions in composite laminates resulting from the development of near-saturation states of transverse cracking, in the absence of other modes of damage.

While the laminate stiffness reduction that results from a given damage state is unique, several damage states may cause the same stiffness reduction. Tensor stiffness evaluations can determine the damage state, provided the dominating damage modes and their locations through the laminate thickness are known. In a more general sense, changes in laminate stiffnesses are merely global manifestations of the changes in stress distributions in the constituent plies resulting from the presence of damage. If lamina properties are reduced in accordance with what is known about the damage modes and a laminate analysis provides reasonable predictions of stiffness in the damaged state, then the in-plane stresses predicted by the laminate analyses are reasonable estimates for stresses in the damaged material. The stresses provided by a laminate analysis in which stress is redistributed via lamina stiffness reduction may provide a basis for predicting strength and life.

REFERENCES

[1] O'Brien, T. K., "Stiffness Change as a Nondestructive Damage Measurement," Mechanics of Nondestructive Testing, W. W. Stinchcomb, Ed., Plenum Press, New York, 1980, pp. 101-121.

[2] Reifsnider, K. L., Henneke, E. G. and Stinchcomb, W. W., "Defect-Property Relationships in Composite Materials," ASML-TR-76-81, Part IV, June 1979.

[3] Reifsnider, K. L., "Some Fundamental Aspects of the Fatigue and Fracture Response of Composite Materials," Proc. 14th Annual Society of Engineering Science Meeting, Lehigh University, Nov. 14-16, 1977.

[4] O'Brien, T. K., "An Evaluation of Stiffness Reduction as a Damage Parameter for Fatigue Failure in Composite Materials," Ph.D. Dissertation, VPI & SU, Oct. 1978.

[5] Camponeschi, E. T., "An Investigation of Stiffness Reduction as an Indicator of Fatigue Damage in Graphite Epoxy Composites," Master's Thesis, VPI & SU, Feb., 1980.

[6] Wang, A. S. D., Law, C. E. Jr. and Warren, W. J., "An Energy Method for Multiple Transverse Cracks in Graphite-Epoxy Laminates," Proc. Winter Annual Meeting of ASME, New York, NY, Dec. 2-7, 1979.

[7] Wang, A. S. D. and Crossman, F. W., "Initiation and Growth of Transverse Cracks and Edge Delamination in Composite Laminates, Part 1, An Energy Method," Drexel University Report, Oct., 1979.

[8] Talug, A., "Analysis of Stress Fields in Composite Laminates with Interior Cracks," Thesis, Doctor of Philosophy, College of Engineering, Virginia Polytechnic Institute and State University, Sept. 1978.

[9] Vasil'ev, V. V., Dudchenko, A. A. and Elpat'evski, A. N., "Analysis of the Tensile Deformation of Glass-Reinforced Plastics," Translated from Mekhanica Polimerov, No. 1, Jan.-Feb. 1970, pp. 144-147.

[10] Zweben, C., "On the Strength of Notched Composites," Journal of Mechanics and Physics of Solids, Vol. 19, 1971, pp. 103-116.

[11] Garrett, K. W. and Bailey, J. E., "Multiple Transverse Fracture in 90° Cross-ply Laminates of a Glass Fibre-Reinforced Polyester," Journal of Materials Science, Vol. 12, 1977, pp. 157-158.

[12] Parvizi, A. and Bailey, J. E., "On Multiple Transverse Cracking in Glass Fibre Epoxy Cross-Ply Laminates," Journal of Materials Science, Vol. 12, 1977, pp. 2131-2136.

[13] Plunkett, R., "Damping in Fiber Reinforced Laminated Composites at High Strain," Journal of Composite Materials Supplement, Vol. 14, 1980.

[14] Tsai, S. W. and Hahn, H., Composite Materials Workbook, Air Force Materials Laboratory Report No. AFML-TR-77-33, March 1977, pg. 195.

[15] Jones, R. M., Mechanics of Composite Materials, McGraw-Hill, New York, 1975.

[16] Stalnaker, D. O. and Stinchcomb, W. W., "Load History-Edge Damage Studies in Two Quasi-Isotropic Graphite Epoxy Laminates," Composite Materials: Testing and Design (Fifth Conference), ASTM STP 674, S. W. Tsai, Ed., American Society for Testing and Materials, 1979, pp. 620-641.

[17] O'Brien, T. K. and Reifsnider, K. L., "Fatigue Damage: Stiffness/Strength Comparisons for Composite Materials," Journal of Testing and Evaluation, JTEVA, Vol. 5, Sept. 1977, pp. 384-393.

[18] Post, D., "Optical Interference Methods for Deformation Measurements--Classical, Holographic and Moiré Interferometry," Mechanics of Nondestructive Testing, W. W. Stinchcomb, Ed., Plenum Press, New York, 1980, pp. 1-53.

APPENDIX I. Determination of the Shear Lag Parameter

As noted in Section 2.3, two material properties that characterize the shear transfer region were required for the implementation of a shear lag analysis. These properties were the shear modulus (G) and the thickness (b) of the shear transfer layer, which appear in the analysis in the form of the shear lag parameter (G/b). Moiré interferometry, an optical technique for determining full-field displacements, was used to determine the shear lag parameter for the glass-epoxy material system used in this investigation.

Moiré interferometry is an optical interference technique: two coherent, collimated beams of light that travel different paths intersect, and a series of light and dark fringes are formed where the two beams cross in space [18]. Light fringes appear where the two beams are in phase and constructively interface, and dark fringes appear where the two beams are out of phase and destructively interfere. In the moiré technique, the difference in the optical path length travelled by the two beams (and thus the difference in phase between the two beams) is changed by in-plane displacement of the specimen surface. Hence moiré fringes are contours of constant relative displacement.

A portion of the moiré fringe pattern from a $[0,90_3]_s$ glass-epoxy specimen with transverse cracks in the 90 deg plies subjected to a longitudinal loading is shown in Fig. 21. The strain distribution between the two cracked sections was determined from the displacement contours provided by the moiré pattern. The shear lag model was used to predict the strain distribution between the cracks using various values

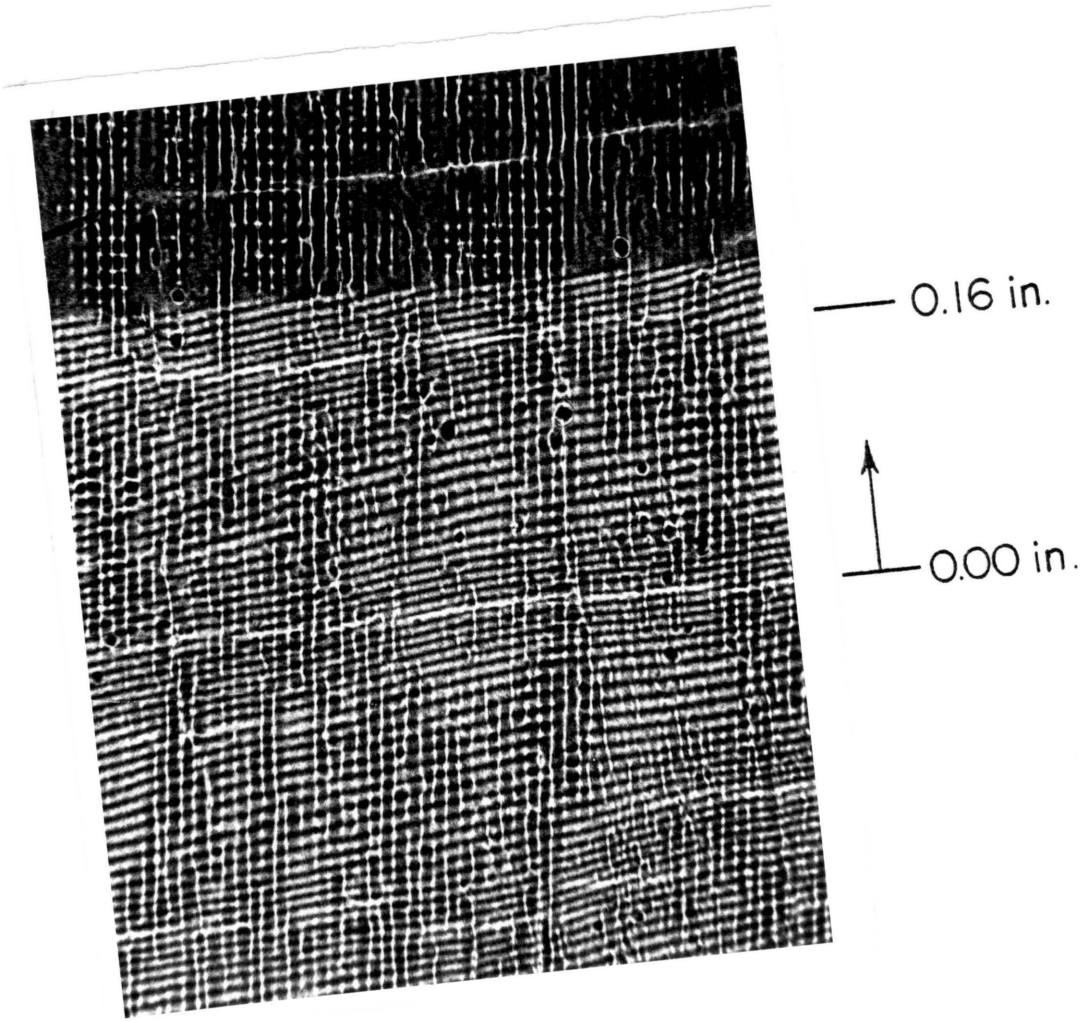

Fig. 21 Moiré fringe pattern of a $[0,90_3]_s$ laminate between cracked sections in the 90° plies.

for the shear lag parameter. The observed and predicted distributions were plotted, and the value of the shear lag parameter was determined by that value for which the predicted distribution of strain most closely matched the observed distribution. By inspection, a value of $(G/b) = 50$ Msi/in. was obtained. Figure 22 indicates that the strain distribution is somewhat insensitive to changes in the shear lag parameter.

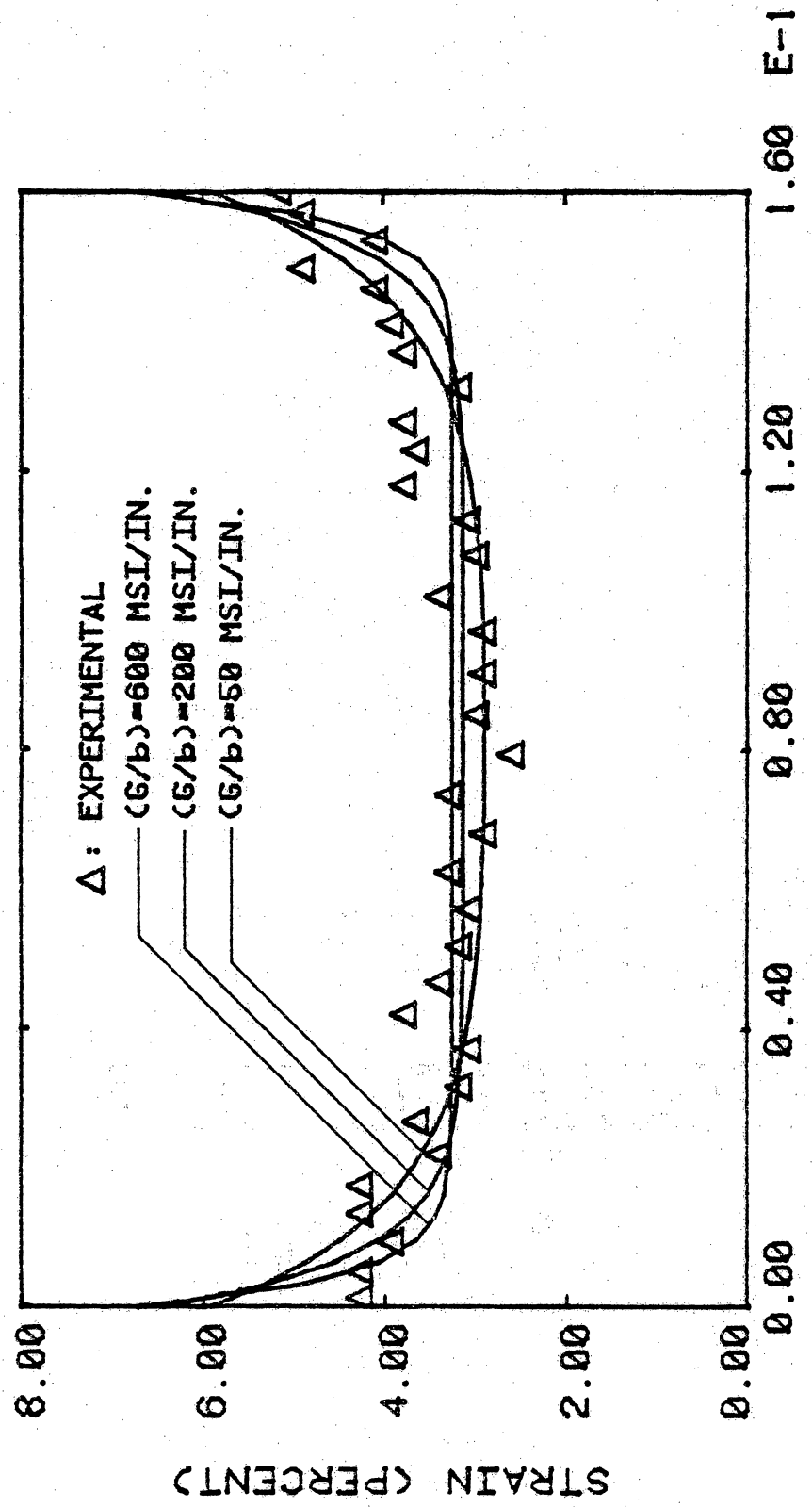

Fig. 22 Predicted and observed strain distributions in the 0° plies of a $[0,90_3]_s$ laminate between cracked sections of the 90° plies.

Appendix II.

Additional Longitudinal Stiffness Evaluation Data

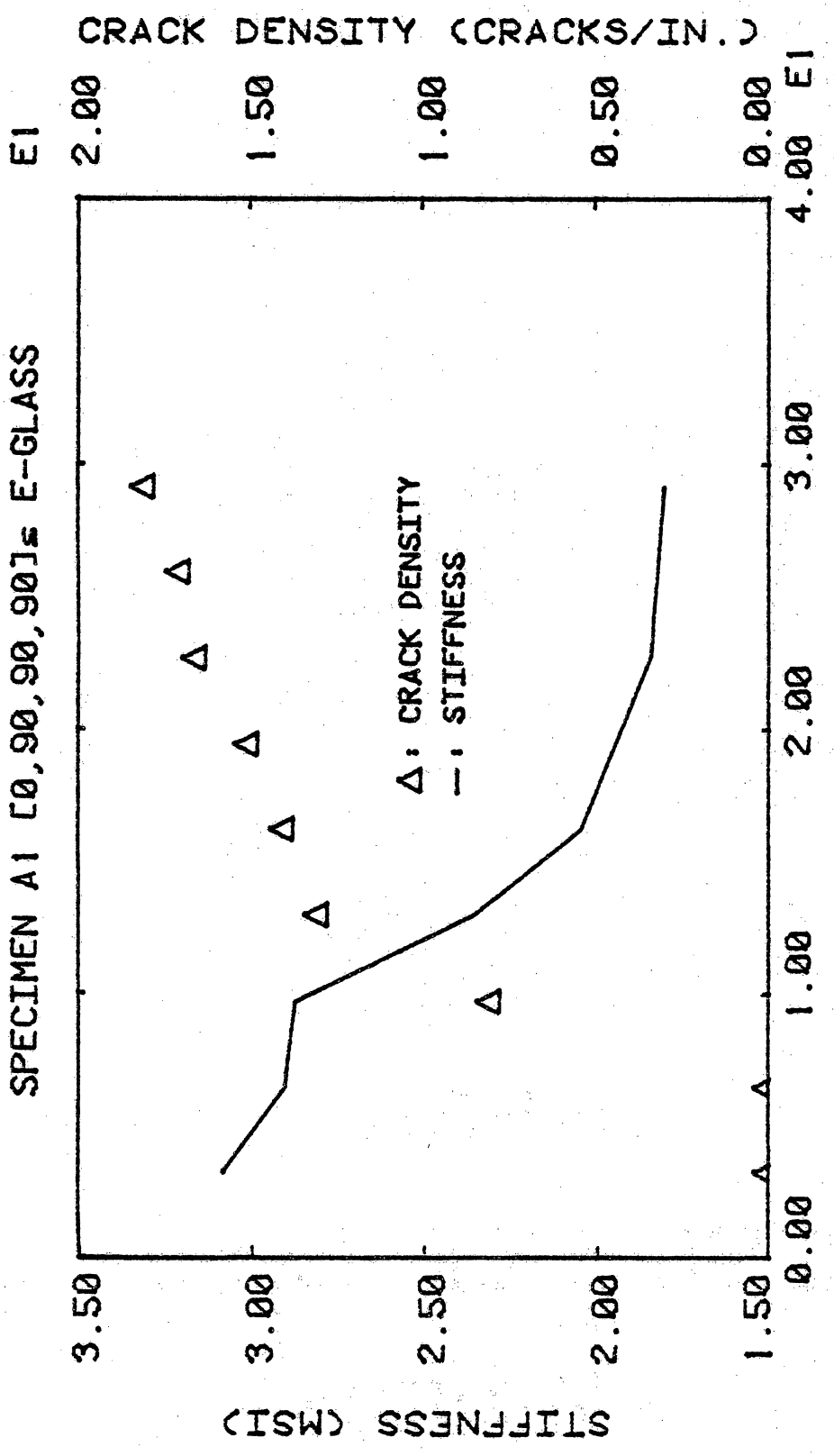

Fig. 23 Stiffness and crack density vs. applied stress for specimen A1.

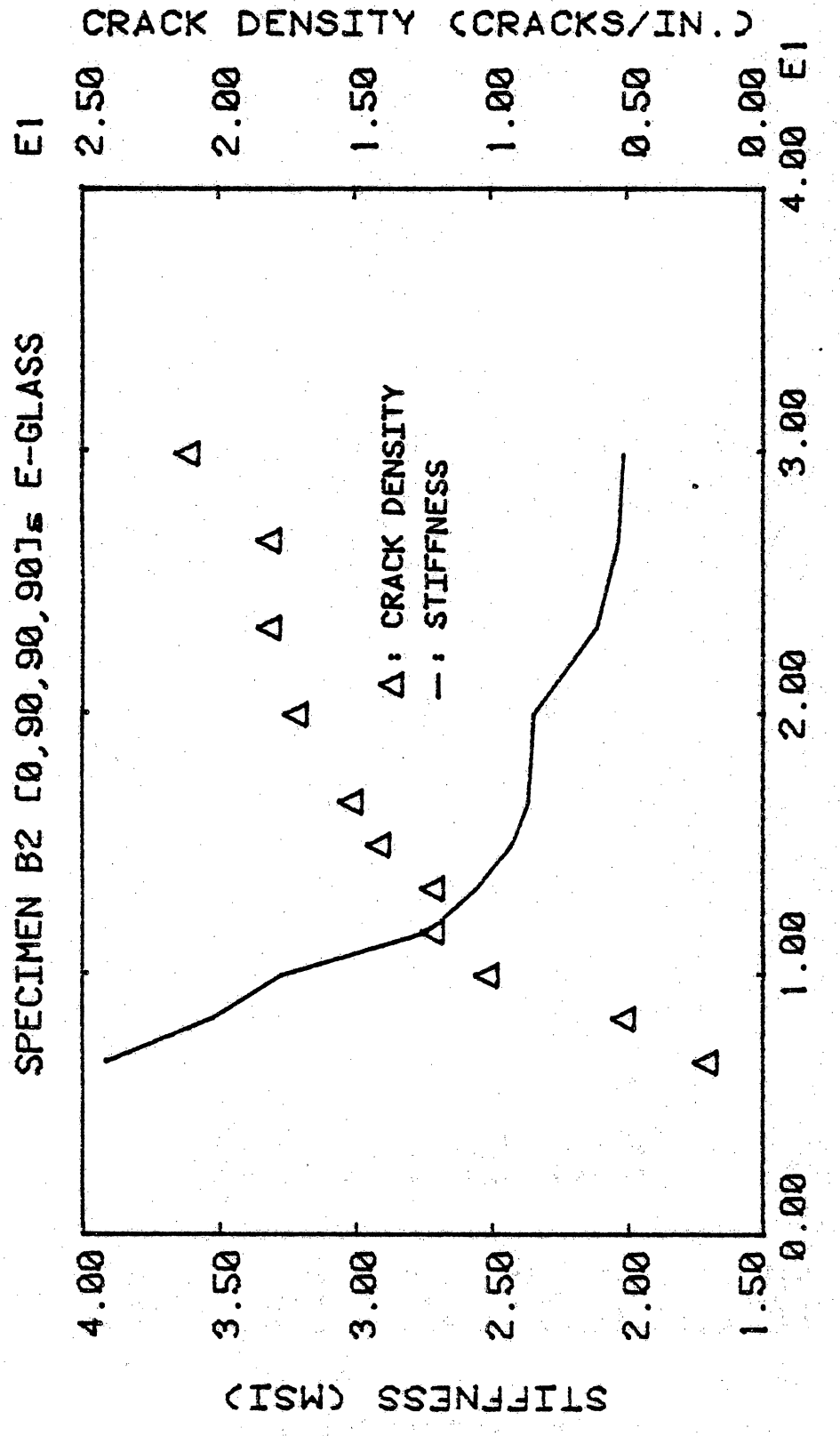

Fig. 24 Stiffness (via strain gage) and crack density vs. applied stress for specimen B2.

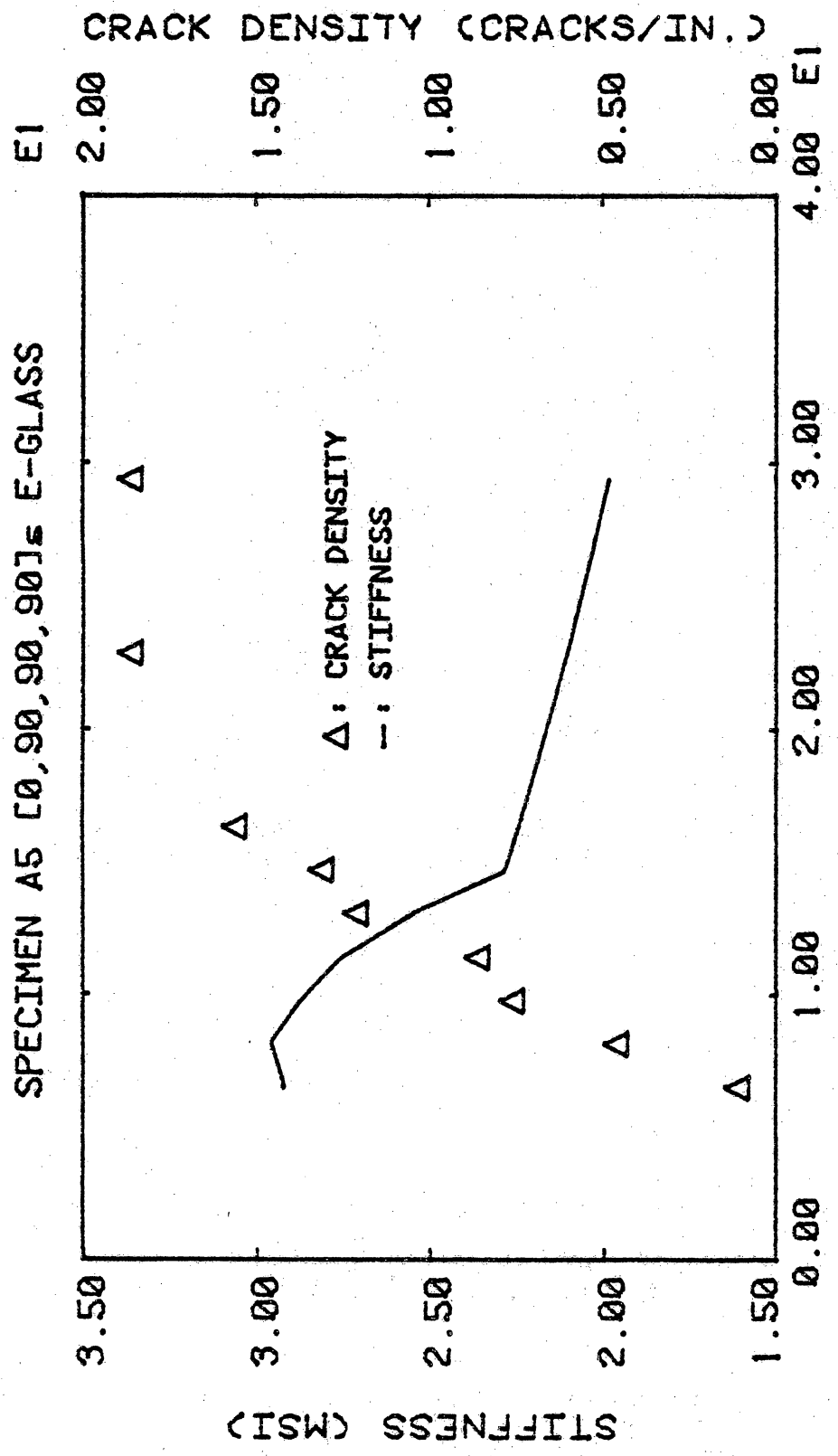

Fig. 25 Stiffness (via strain gage) and crack density vs. applied stress for specimen A5.

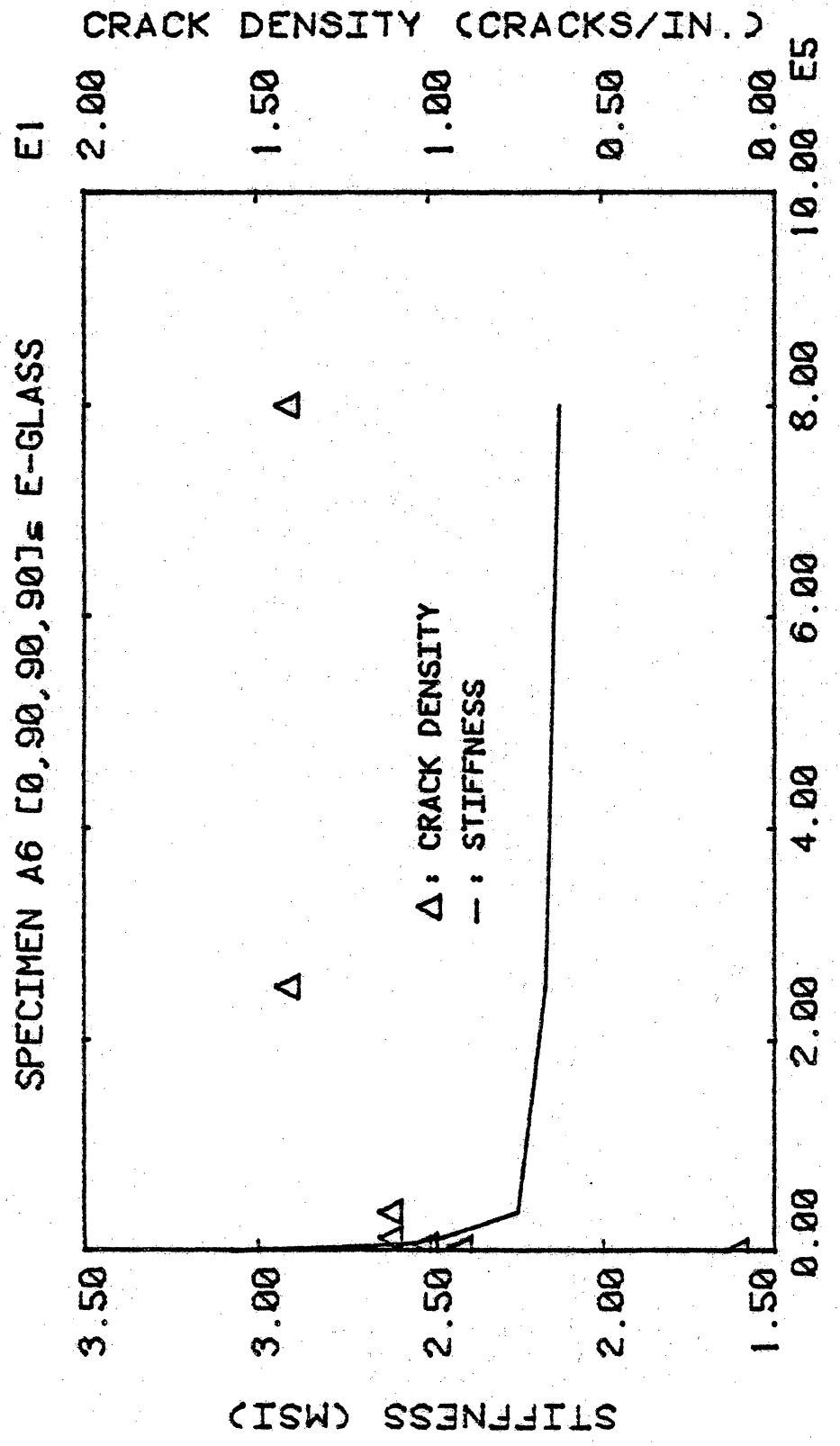

Fig. 26 Stiffness and crack density vs. cycles of loading for specimen A6 (σ_{max} = 0.20 σ_{ult}, R=0.1).

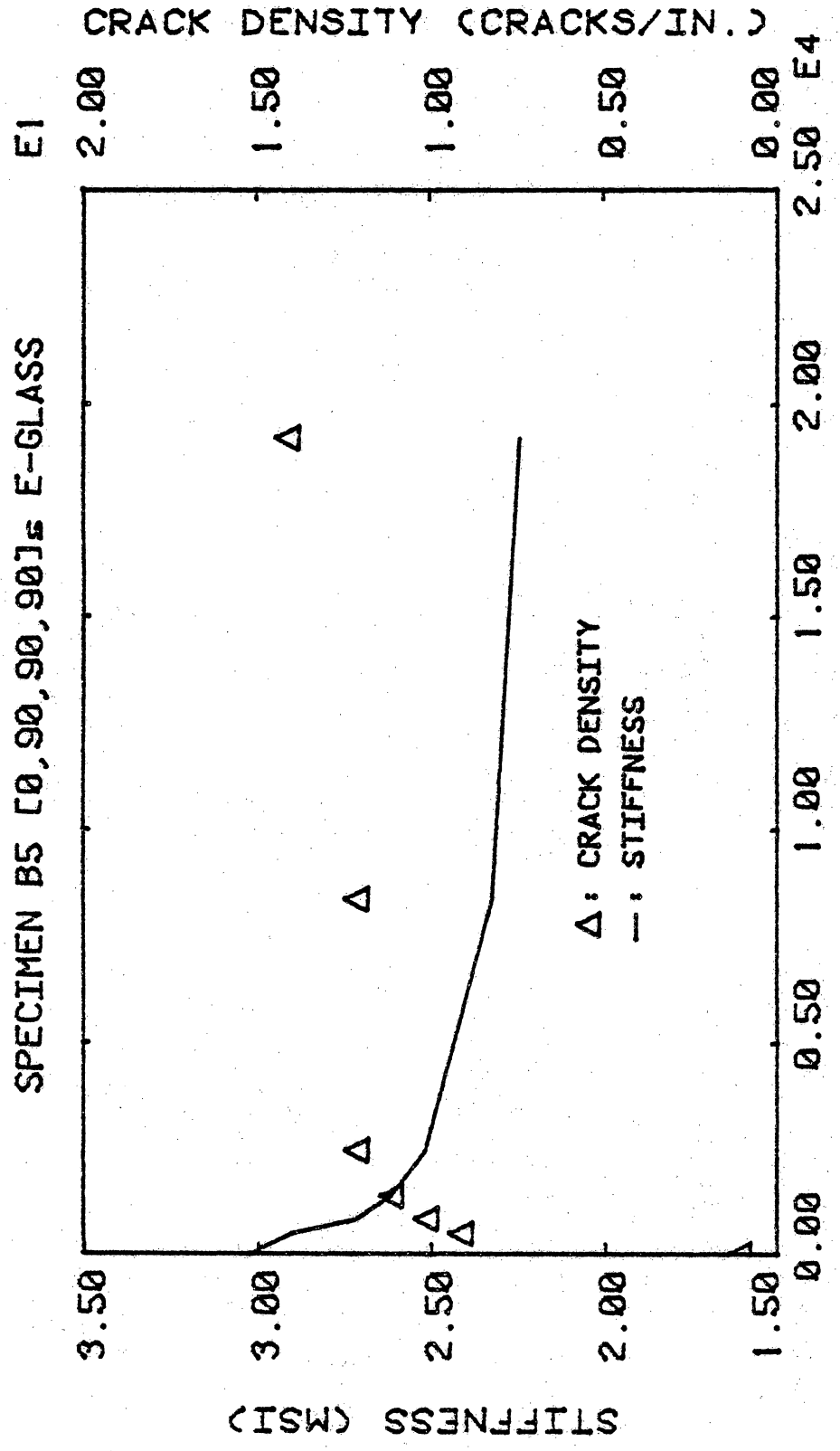

Fig. 27 Stiffness and crack density vs. cycles of loading for specimen B5 ($\sigma_{max} = 0.20\ \sigma_{ult}$, R=0.1).

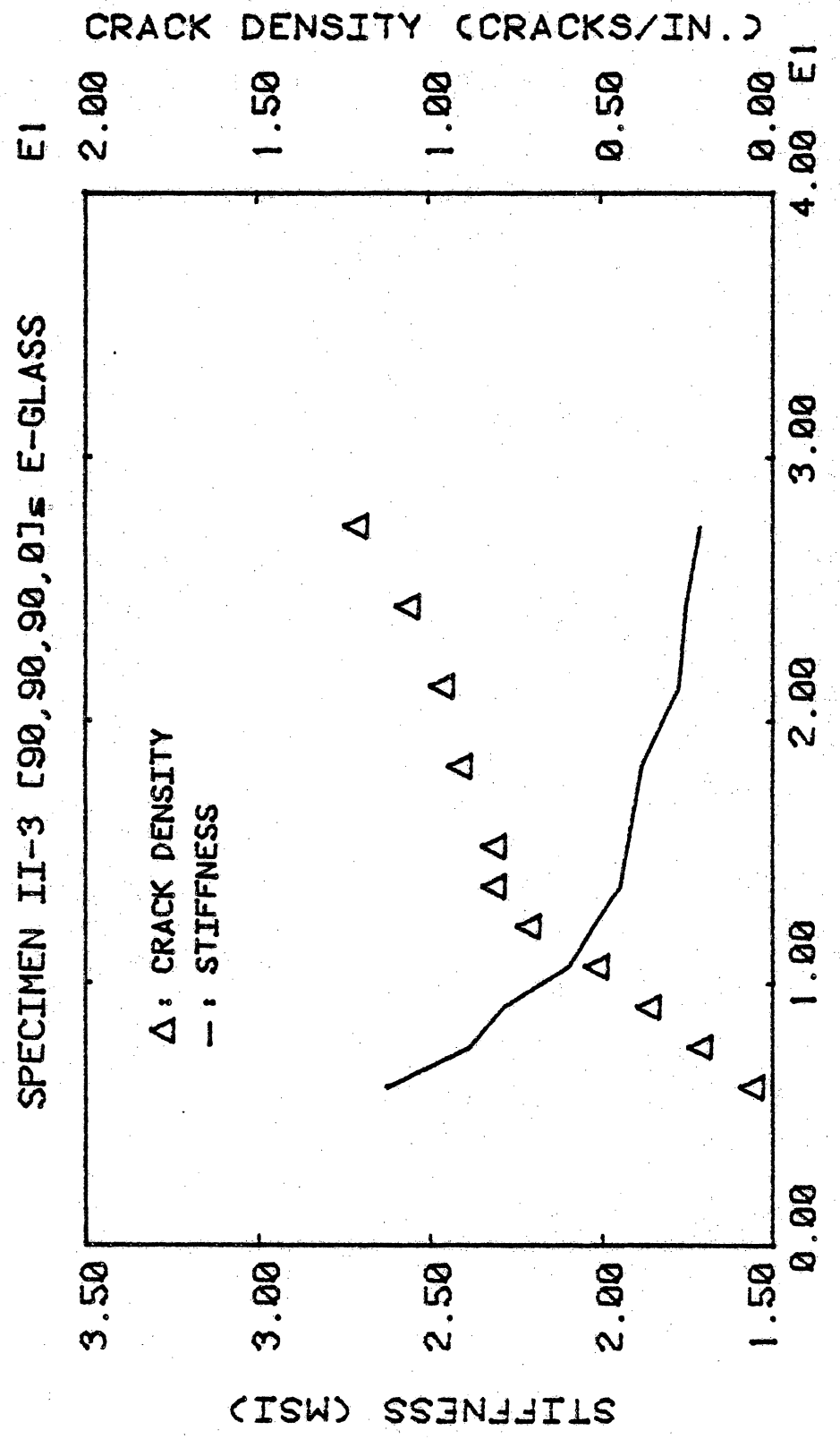

Fig. 28 Stiffness and crack density vs. applied stress for specimen II-3.

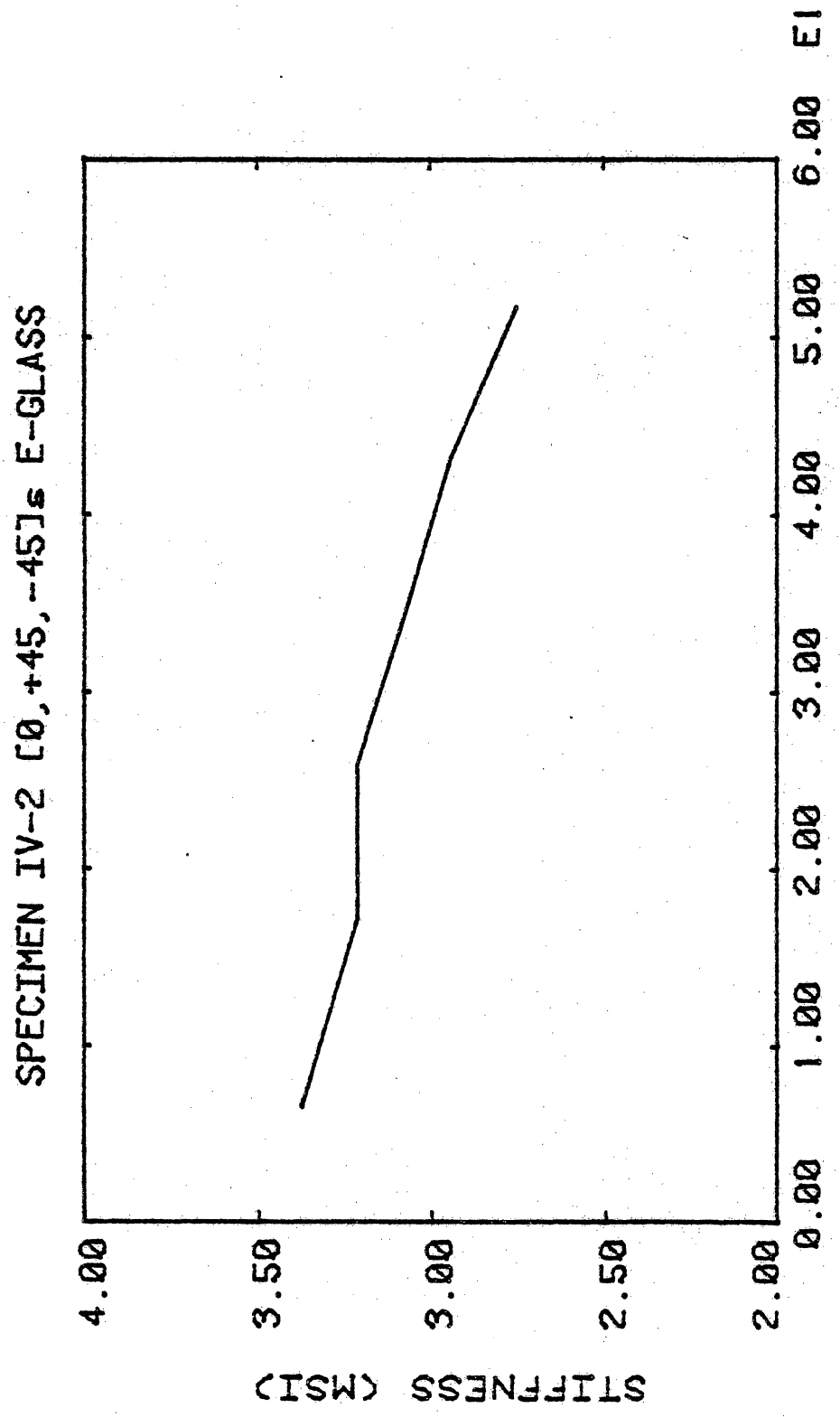

Fig. 29 Stiffness vs. applied stress for specimen IV-2.

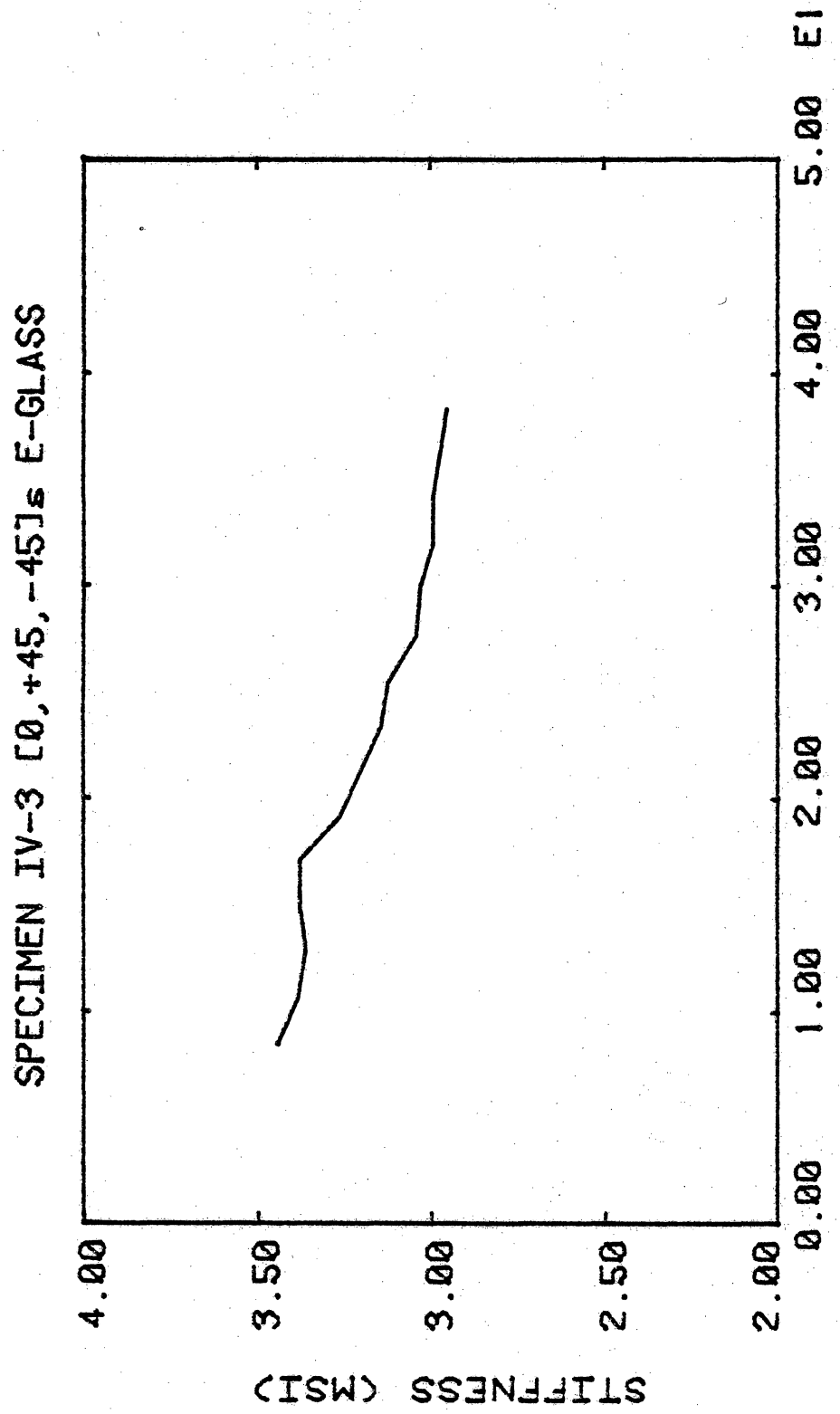

Fig. 30 Stiffness vs. applied stress for specimen IV-3.

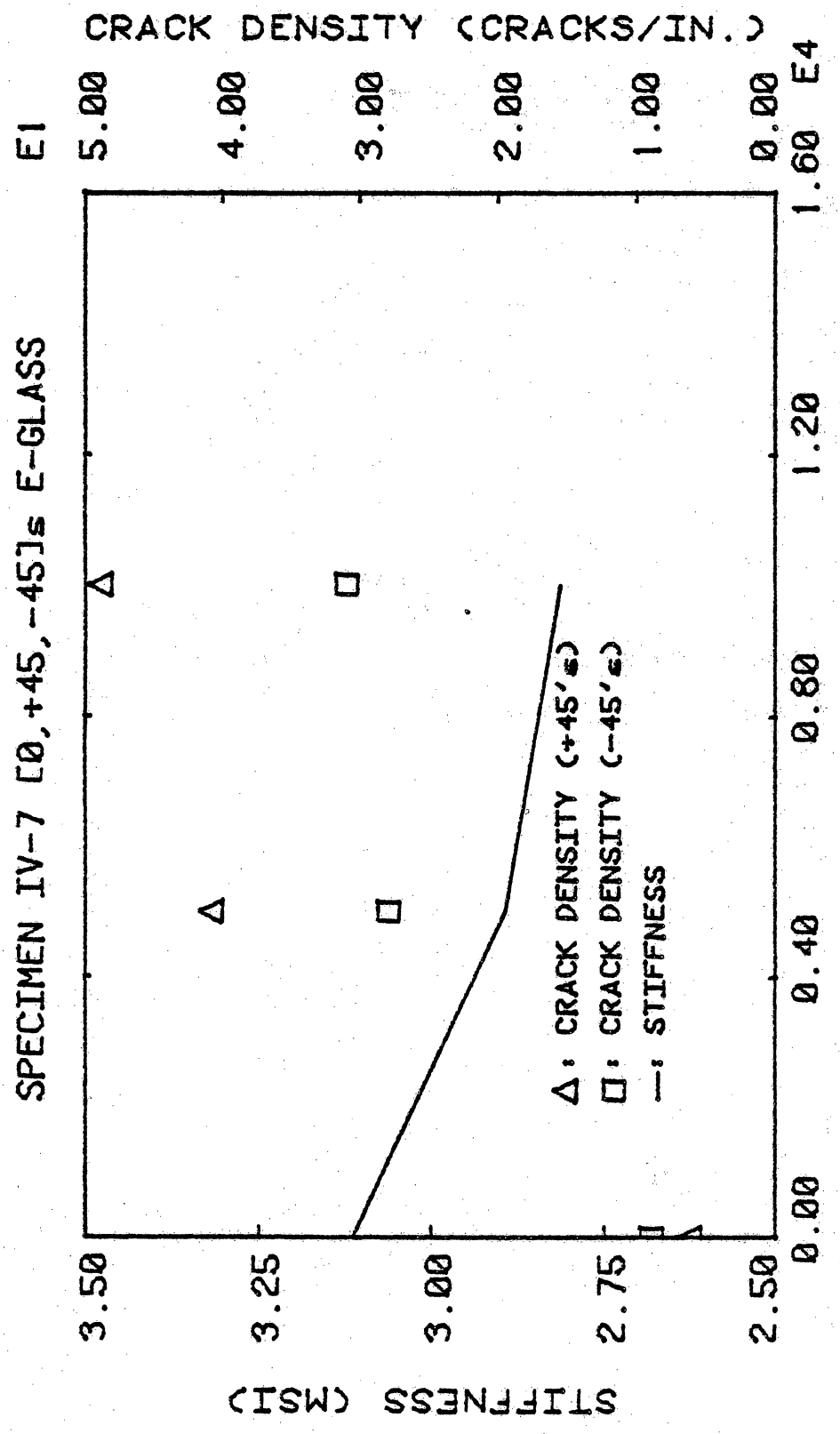

Fig. 31 Stiffness and crack density vs. cycles at loading for specimen IV-7 ($\sigma_{max} = 0.60\ \sigma_{ult}$, R=0.1).

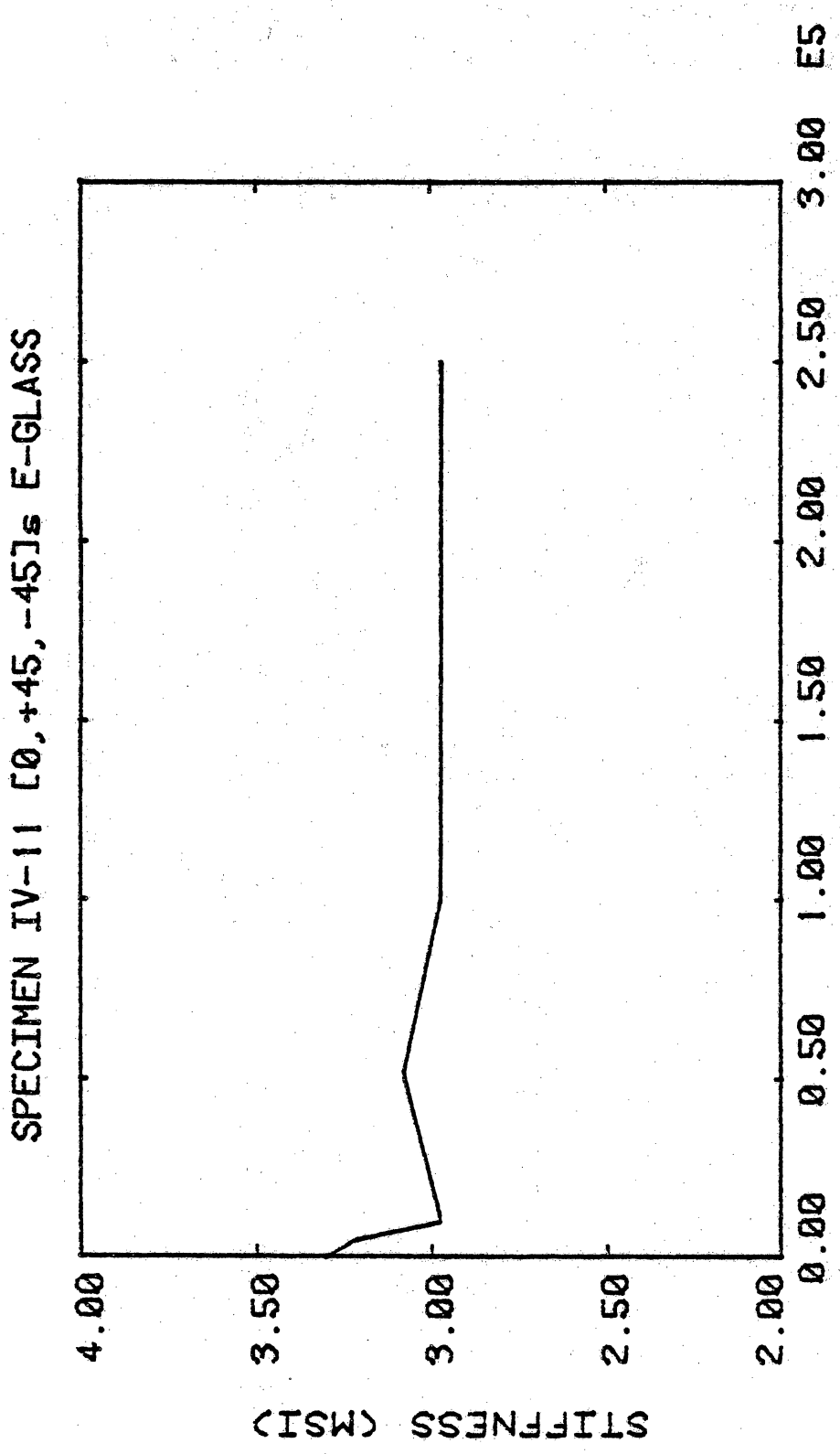

Fig. 32 Stiffness vs. cycles of loading for specimen IV-11 (σ_{max} = 0.35 σ_{ult}, R=0.1).

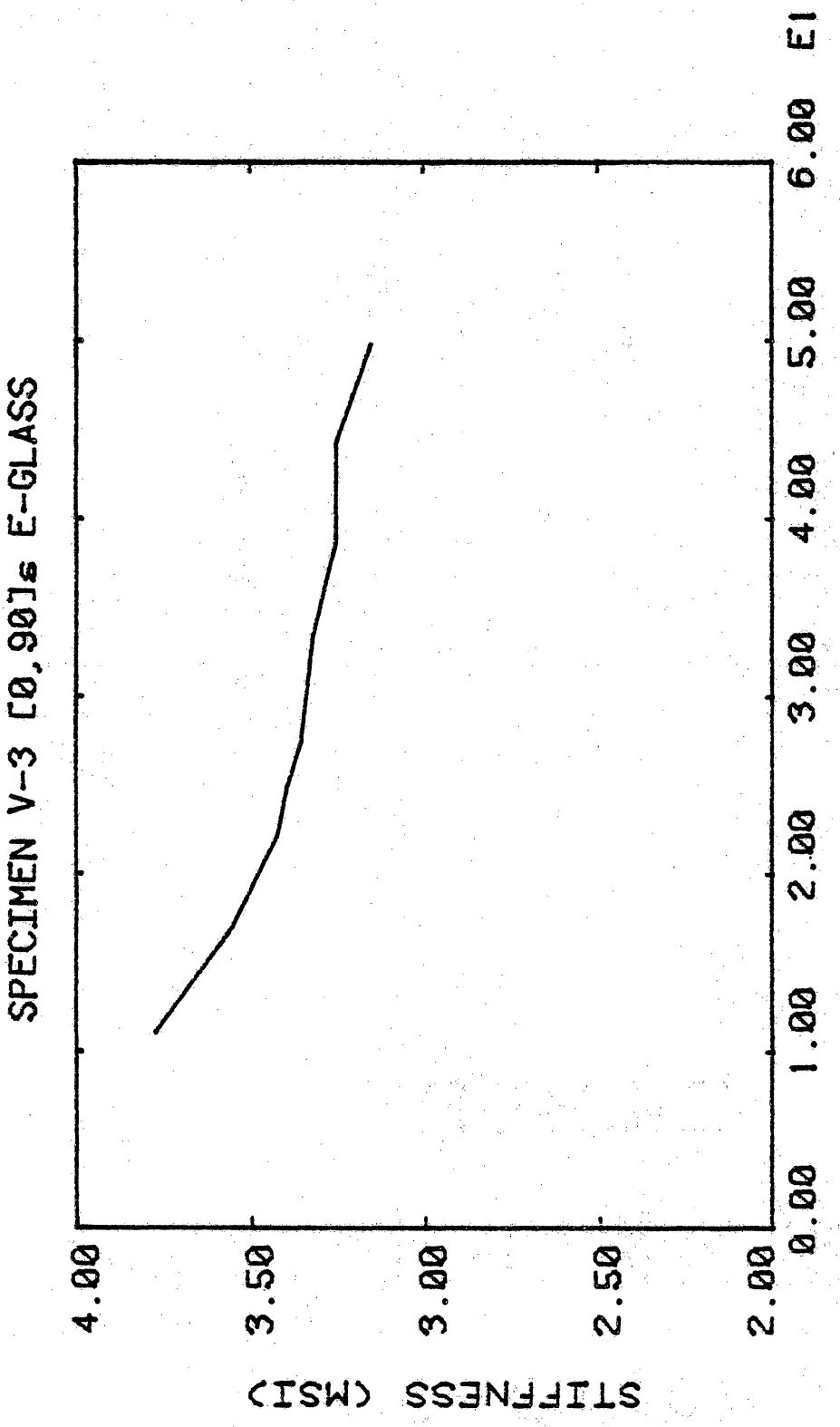

Fig. 33 Stiffness vs. applied stress for specimen V-3.

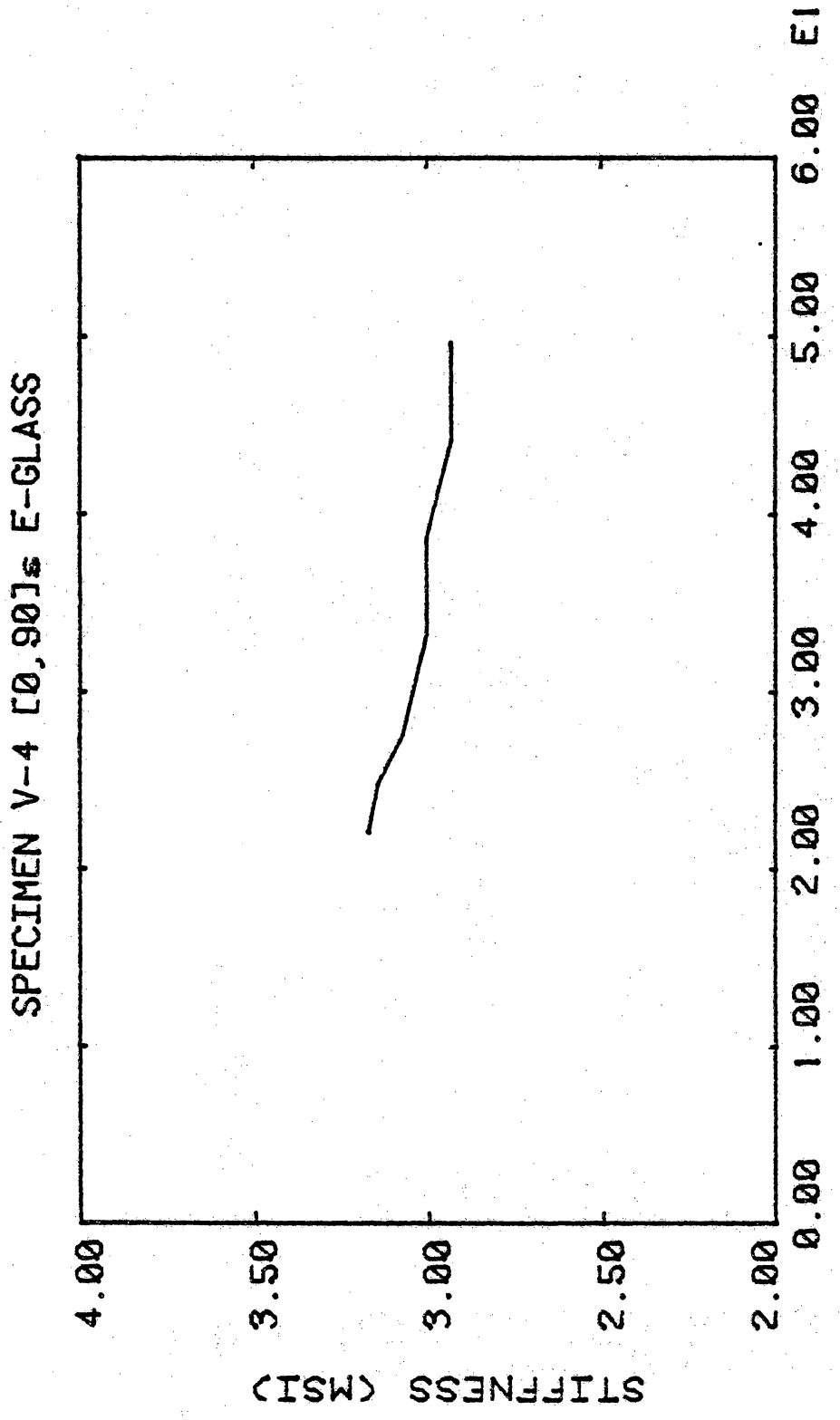

Fig. 34 Stiffness vs. applied stress for specimen V-4.

The vita has been removed from the scanned document

STIFFNESS REDUCTION RESULTING FROM TRANSVERSE CRACKING IN FIBER-REINFORCED COMPOSITE LAMINATES

by

Alton Lee Highsmith

(ABSTRACT)

Several damage modes, including fiber breakage, delamination, and transverse cracking, have been observed to contribute to the mechanical degradation of fiber-reinforced composite laminates. In this investigation, the effect of transverse cracking on laminate stiffness was studied. Four glass-epoxy laminates ($[0,90_3]_s$, $[90_3,0]_s$, $[0,90]_s$, and $[0,\pm45]_s$) were evaluated.

Two experimental test sequences were performed. In the first test sequence, longitudinal stiffness was measured at various stages of damage development. Damage development was monitored via edge replication. In the second test sequence, four laminate stiffnesses (E_{xx}, ν_{xy}, G_{xy}, and D_{yy}) were measured in the undamaged and near-saturation damage states.

Two analytical models were evaluated. A one dimensional shear lag model was used to predict longitudinal stiffness as a function of crack density for the $[0,90_3]_s$ and $[90_3,0]_s$ laminates. Correlation between theory and experiment was good. A modified laminate analysis was used to predict four laminate stiffnesses (E_{xx}, ν_{xy}, G_{xy}, and D_{yy}). Except for the $[0,\pm45]_s$ case, a laminate in which significant amounts of damage other than transverse cracking were observed, agreement between predicted and observed stiffness changes was good.